SOL-GEL-PLATFORM OPTICAL SENSORS FOR OXYGEN GAS: SENSOR DEVELOPMENT AND INVESTIGATION OF PROBE PARTIONING IN SOL-GEL MATRICES

By

Desirée L. Plata

****

Submitted in partial fulfillment
of the requirements for
Honors in the Department of Chemistry

UNION COLLEGE

June, 2003

ABSTRACT

PLATA, DESIREE L. Sol-gel-platform optical sensors for oxygen gas: sensor development and investigation of probe partitioning in sol-gel matrices. Department of Chemistry, June 2003.

I have developed gas sensors that respond rapidly and noticeably to changes in oxygen concentration by doping fluorescent complexes into gas-permeable sol-gel materials. Ruthenium (II) 4,7-diphenyl-1,10- phenanthroline, $Ru(dpp)_3^{2+}$, responds to variations in ambient oxygen concentrations through marked changes in its fluorescence intensity. I investigated the response of $Ru(dpp)_3^{2+}$ to oxygen in solution, in xerogels (sol gels dried under ambient conditions) and in aerogels (sol gels dried using supercritical conditions). Aerogels have particularly high porosity and low density, which allows for rapid diffusion of gases into the material. The aerogel sensor responds reversibly to changes in ambient oxygen concentration within 10 s, as compared to 50 s for $Ru(dpp)_3^{2+}$ in a xerogel and a 69-min. response time in solution. These rapid, reversible systems have potential for use as switches, and future work will focus on evaluating their use as quantitative oxygen sensors. In addition, I have conducted fluorescence lifetime measurements to monitor probe partitioning within the aerogels and xerogels, in order to ascertain whether there are fundamental differences in the microenvironments experienced by the probes in the two types of sol gels. I have found that the probes exist in two distinct microenvironments (presumably, within the silicate matrix and along the pore-matrix interface region) within both types of sol-gel materials. This indicates that probe partitioning likely occurs early on in the sol-gelation process.

Table of Contents

Table of Figures

Table of Tables

Introduction

Ambient gas concentrations have substantial affects on many chemical processes that impact daily human activity, such as the weather, breathing rates, and corrosion. The ability to detect changes in the composition and flow rates of air is important for forensic, military, mechanical, chemical, environmental, and health considerations, to name a few. While humans have rather highly developed physiological capabilities to detect these changes, we are limited by the range, ability to identify, quantification, and speed of detection of gaseous compounds.[1,2] Indeed, many deaths were attributed to carbon monoxide poisoning in the 1940s due *to ex-post facto* leak detection in natural gas home heating systems.[3] An ideal gas detector would respond rapidly and noticeably to a specific analyte at low concentrations. In order to achieve these prerequisites, one must have a probe whose properties change in an observable fashion in response to ambient changes in analyte concentration, and that probe must have rapid accessibility to a bulk sample of the fluid of interest. We have coupled an oxygen-sensitive molecular probe to a low-density material, through which air can diffuse rapidly and, in doing so, developed an oxygen sensor with potential for multiple and versatile applications.

Highly porous materials can be formed by the extensive polymerization reactions of metal alkoxides. Such hydrolysis and condensation polymerization reactions initially produce gel-like structures, so they are referred to as sol-gel processes. Silicate precursors, such as tetramethyl orthosilicate ($Si(OCH_3)_4$, TMOS), are commonly used to produce silica glasses by the following reactions[4]:

$$Si(OCH_3)_4 + 4H_2O \rightarrow Si(OH)_4 + 4CH_3OH \quad \text{(hydrolysis)}$$
$$n\,Si(OH)_4 \rightarrow nSiO_2 + 2n\,H_2O \quad \text{(condensation)}$$
} polymerization

The resultant material is a highly crossed linked polymer matrix, whose pore space is filled with solvent, as shown in Figure 1. This solvent can be evacuated from the pore-matrix either by evaporation or by supercritical extraction; the two methods yield composites with different physical properties. During solvent evaporation, the surface tension, which exists at any liquid-gas interface, exerts a force large enough to collapse the pore structure until the gel network becomes strong enough to resist this compressive force.[5] This generates a condensed silicate matrix, referred to as a xerogel, which is made up of 60-90% air[3], with a pore diameter of 1-20 nm.[5] Evacuating the solvent above its critical point, where neither liquid nor gas is present, can eliminate the surface tension, as it eliminates the liquid-gas interface. The solvent leaves the pore structure as a supercritical fluid, which shares some properties of a liquid and some properties of a gas. Consequently, the pore structure does not collapse, but is instead maintained, yielding a low-density solid known as an aerogel.[7] Referred to as "solid clouds," aerogels typically consist of 90-99% air[6], with pore diameters from 1-50 nm.[5]

In general, four different microenvironments exist within a sol-gel matrix: (1) the pore space, (2) within the silicate matrix, (3) along the pore-matrix interface, and (4) the constraining region, where the distance between the pore walls is roughly the diameter of a probe complex. Three of these regions are depicted in Figure 2.

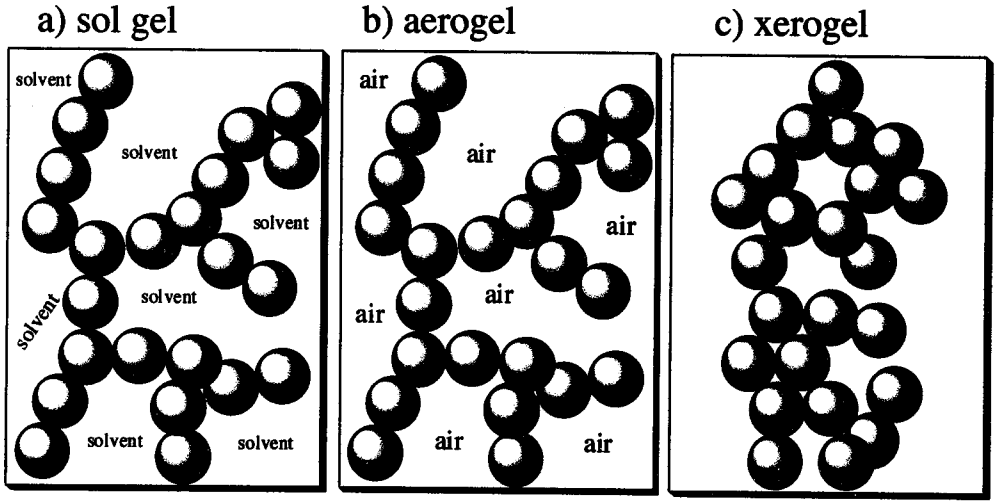

Figure 1. Microstructure of sol-gels, xerogels, and aerogels. **(a) Sol-gel** matrices contain solvent-filled pore spaces. **(b)** Drying a sol gel under ambient conditions gives a **xerogel**, whose pore structure is condensed as a result of the compressive force of solvent surface tension during evaporation. **(c)** Supercritical drying of a sol gel eliminates surface tension during solvent evacuation, so the pore nanostructure is maintained, producing an **aerogel.** This figure was modified from artwork in Brinker & Scherer[5].

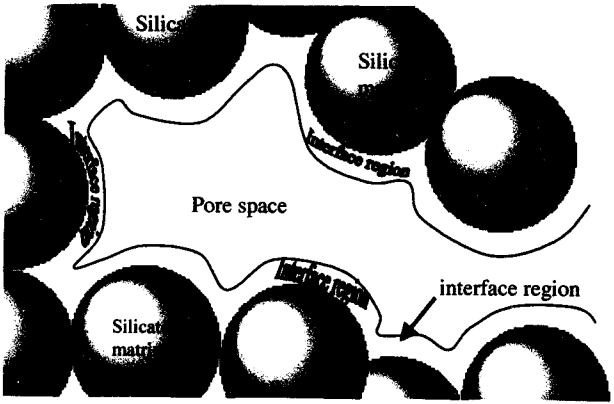

Figure 2. Schematic of three important regions within the sol-gel matrix. The gray spheres represent the surface of the silicate polymer matrix. The pore space, pore-matrix interface, and silicate matrix are shown. The constraining region is not shown. Figure modified from Dunn & Zink[4].

Aerogels have the lowest known density, index of refraction, thermal, electrical, and acoustical conductivities of any solid material[5,7]. Since they are fabricated from a liquid to form a solid, their geometry can be easily manipulated. In addition, they resist changes in structure over time and exhibit tensile strengths of 16kPa or higher[8]. The combination of these exceptional properties in one material makes the development of aerogel applications a very exciting and broad field of study. Currently, aerogel technology is being employed for use in radiation detectors, electronics, thermal insulators, insulated windows, comet dust collection, nuclear waste storage, hydrocarbon remediation, batteries, affinity columns, drug screening platforms, bioanalytical sensors and more.[7,9]

Since their discovery in the 1940s and 1950s by Peter Kistler,[10] the development of aerogels has been limited by the cost, risk, and time associated with their production. In 2001 and 2002, a novel rapid supercritical extraction (RSCE) method was developed at Union College that has improved safety, decreased cost and equipment requirements, and decreased preparative work. Essentially, to form an aerogel, one only needs to mix a solution of precursors, pour the solution into a mold between two hot-press platens, press a button, and return ten hours later.[8,11] During the ten-hour fabrication process, the temperature within the mold is raised beyond the critical temperature of the solvent (methanol), and the hot press provides a restraining force against the rising pressure. When the pressure on the mold is released, the solvent evacuates the sol-gel pore space as a supercritical fluid, leaving behind a porous aerogel matrix. In addition, it has been demonstrated that fluorescent probes (Figure 3) are successfully entrapped in the silicate

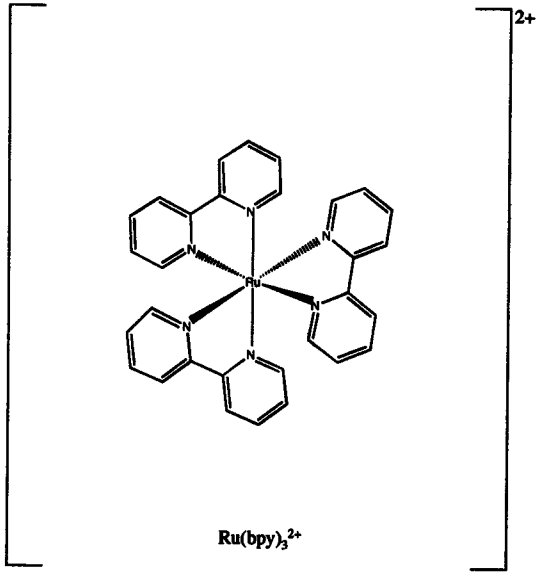

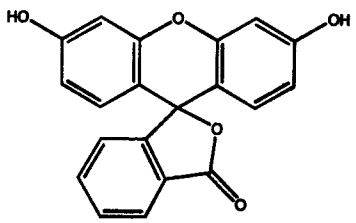

Fluorescein

Figure 3. Fluorophores successfully incorporated into aerogels. The complex on the left is tris(2,2'-bipyridyl)ruthenium(II) (Ru(bpy)$_3^{2+}$) a popular organometallic flurophore. The molecule on the right is fluorescein, which is better known as yellow no. 7.

matrix using the Union RSCE method simply by adding a solution containing the fluorophore to the mixture of sol-gel precursors prior to gelation.[12]

We are able to exploit these molecular species as probes because they exhibit characteristic spectroscopic properties that change in response to their environment. A charged particle, such as an electron, is able to absorb energy from the electric field of a light wave, provided that the energy from that wave matches the energy between two quantized energy levels within a molecular species.[13] Upon absorbing the energy from the incident light, the species will be promoted from the ground state, S_0 (lowest energy configuration, electron spins paired), to the singlet state, S_1.[13,14] The lowest possible energy is the favored state of existence for any molecular species, and so, an excited molecule will relax back to the ground state, and can do so through several processes.

An excited molecular species can relax to the lowest vibrational energy level within an electronically excited singlet state (S_1, S_2) by vibrating and colliding with other molecules. This is called vibrational relaxation. Internal conversion occurs when an excited species drops to a lower electronic energy level, and is a common mode of relaxation when there are many vibrational states associated with a given singlet state. Rigid molecules, such as aromatic compounds, have fewer vibrational degrees of freedom, and therefore relax via alternate paths. A common path of relaxation of aromatic molecules is fluorescence, during which a molecule will emit visible or ultraviolet light. Fluorescence occurs when a molecule drops from the lowest vibrational energy level of the singlet state to any vibrational energy level of the ground state.

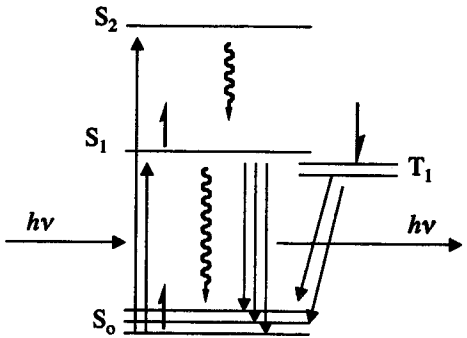

Figure 4. Jablonski Diagram depicting the modes of relaxation from an electronically excited state. Fluorescence is represented by the blue arrows. During fluorescent relaxation, a photon is given off. Other modes of relaxation are non-radiative, such as internal conversion, which is represented by the squiggle arrows. Figure modified from Sharma and Schulman.[13]

Molecules can drop in energy from the singlet state to the triplet state (T_1, excited energy state, parallel spin as ground state electron). Relaxation from this triplet state is known as phosphorescence.[12,13]

One parameter with which we can characterize fluorescence is fluorescence lifetime (τ) decay, the average time it takes for an excited molecule to return to the ground state. As fluorescence is only one of several possible modes of relaxation, the fluorescence lifetime of an excited molecule is affected by the rate of decay from the excited state via all of the relaxation pathways. The percent contribution of each relaxation mode changes depending on the state of the probe, its surroundings, and its interactions with other molecules. Presumably, the average lifetime of fluorescence is shortened with increased collisional interactions, and shorter lifetimes are often observed in more constrained systems. Therefore, we can gain information about a fluorophore's environment by measuring its lifetime.

If a fluorophore partitions into multiple microenvironments within a sample, it will exhibit multiple lifetimes. The contribution of each lifetime is characterized by pre-exponential factors, A_1 and A_2. These are shown in Equations 1 and 2, which describe mathematical fits to exponential fluorescence decay curves for first-order (one lifetime) and second-order (two-lifetimes) decay, respectively. The success of these fits is given by a $\chi 2$ value; the closer the value to unity (1), the better the fit.

(1) $I(t) = A_1 e^{(-\tau_1 t)}$

(2) $I(t) = A_1 e^{(-\tau_1 t)} + A_2 e^{(-\tau_2 t)}$,

where I(t) is the luminescence intensity at time t, and τ_1 and τ_2 give the decay rate constants.

Luminescence intensity is a direct measurement of the amount of fluorescence of a molecule. It is proportional to the intensity of the source light as well as the probability of absorption of light by the fluorophore. Hence, fluorescence intensity increases with respect to fluorophore concentration. Molecules that decrease the fluorescence intensity by deactivating excited molecules through molecular collisions are known as fluorescence quenchers. Oxygen, halogens, amines, and electron-deficient molecules often act as efficient quenchers.[14]

The intensity of fluorescence is also dependent on the wavelength of light used to excite the molecule, as the incident light must match the energy of an electronic transition in order to be absorbed by a molecule. By exciting a molecule over a wide range of wavelengths and measuring the subsequent fluorescence, one obtains an excitation spectrum that clearly indicates the optimal wavelengths over which one can excite a given fluorophore. Fixing the excitation wavelength, one can monitor the relationship between the emission wavelength and the fluorescence intensity. That is, one can find the wavelength at which the molecule emits energy most strongly. These emission and excitation spectra are characteristic of fluorescent species. The fluorescence spectra of some molecular species change with respect to the environment. Systems that decrease the energy spacings of the fluorescent complex will will give red-shifted spectra (intensity peaks shift to higher wavelengths), while environments that increase the energy

spacings of the fluorescent complex give blue-shifted spectra (intensity peaks shift to lower wavelengths).

As fluorescence spectral properties are dependent on the energetics of the fluorophore environment, we can investigate matrix-probe interactions, surface chemistry, internal solvent dynamics, and ambient analyte concentrations by monitoring changes in fluorescence spectra and fluorescence decay.

Ruthenium (II) 4,7-diphenyl-1,10-phenanthroline ($Ru(dpp)_3^{2+}$) is a highly conjugated colored complex. Due to its extensive conjugation, it has a constrained conformation, and we can therefore expect that it will fluoresce strongly. We aimed to incorporate this fluorescent moiety into an aerogel matrix. The remarkably low density of the silicate network should allow for rapid diffusion of air into the solid, giving the probe immediate access to the sample of interest. We then investigated the potential use of the $Ru(dpp)_3^{2+}$-doped aerogel as an oxygen sensor.

We established the successful incorporation of the probe into the matrix. We then investigated the speed and sensitivity of the detector to ambient oxygen concentrations, probing the reversibility, linear response range, and specificity of the sensor. In addition, we characterized the spectral properties of the molecular probe in aerogels, xerogels, and solutions, broadening our knowledge of the sol-gel matrix-probe interactions. This work yielded a sensor that is cost- and time-effective, requiring little synthetic work, and can be easily adapted for simultaneous use with many of the current aerogel systems.

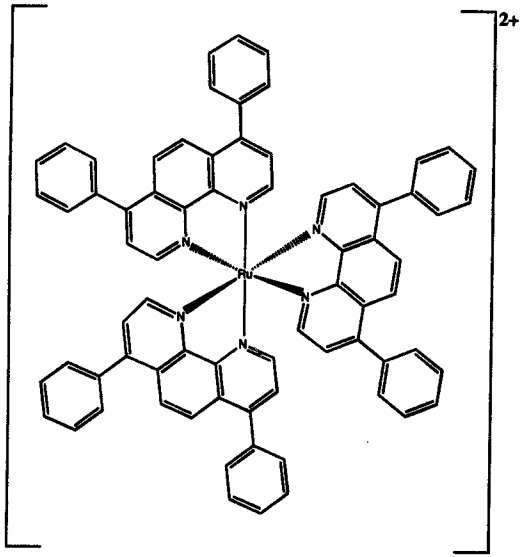

Figure 5. Ruthenium (II) 4,7-diphenyl-1,10-phenanthroline ($Ru(dpp)_3^{2+}$). An oxygen-sensitive, oranometallic probe complex.

Experimental

Materials

Tetramethyl orthosilicate (TMOS) was purchased from Sigma-Aldrich at 98% purity. The $[Ru(bpy)_3]^{2+} \bullet 6\ H_20 + 2Cl^-$ dye was purchased from Strem Chemicals at 98 % purity. Solutions of $[Ru(bpy)_3]^{2+}$ were prepared in deionized water. The $[Ru(dpp)_3]^{2+} \bullet 6\ H_20 + 2Cl^-$ dye was purchased from GFS Chemicals at an unlisted purity (the manufacturer noted that the sample passed the UV-vis spectrophotometry test). All $[Ru(dpp)_3]^{2+}$ solutions were prepared using absolute ethanol (CH_3CH_2OH, EtOH), unless otherwise noted. Fine porosity, slow flow rate filter paper used in the $[Ru(dpp)_3]^{2+} \bullet 6\ H_20 + 2Cl^-$ purification process was purchased from Fisher Scientific.

Preparation of $Ru(dpp)_3^{2+}$ solutions, xerogels, & aerogels

The $[Ru(dpp)_3]^{2+} \bullet 6\ H_20 + 2Cl^-$ solid was purified by washing with chilled, distilled deionized water using fine-grade filter paper, as suggested by Cho and Bright.[15] The filtrate was retained for spectral analysis. After drying under ambient conditions, a 1.0×10^{-3} M $Ru(dpp)_3^{2+}$/ EtOH stock solution was prepared by dissolving 0.0117 g $[Ru(dpp)_3]^{2+} \bullet 6\ H_20 + 2Cl^-$ in 10.0 mL of absolute EtOH. Additional EtOH solutions of varying $Ru(dpp)_3^{2+}$ concentration, ranging from 2.5×10^{-7} to 1.0×10^{-4} M, were prepared by dilution of the stock solution. The solutions used to collect excitation and emission spectra of the $Ru(dpp)_3^{2+}$ solutions were prepared in regular grade EtOH, whereas all other solutions were prepared using absolute EtOH.

The xerogels were prepared by Smitesh Bakrania in the Union College Mechanical Engineering Department who made a sol-gel solution containing 27.5 ml TMOS, 8.5 ml

Methanol (MeOH), 3.6 ml of the desired $Ru(dpp)_3^{2+}$ solutions, and 0.1 ml 1.5 M ammonia (NH_4OH), pouring that solution into polystyrene cuvettes, and then allowing the xerogels to dry under ambient conditions. Over a period of two to four weeks, the xerogels shrunk in volume by roughly 40–60%. This change in size results from the collapse of the pore structure, which is caused by the surface tension of the evaporating solvent.

The aerogels were prepared by Smitesh Bakrania by the Union Rapid Supercritical Extraction Method (RSCE)[8,11] and the above sol-gel solution. This method employs a hot press to manipulate the temperature and pressure during the sol-gelation process, thereby extracting the pore-space solvent as a supercritical fluid and preventing the collapse of the pore structure. The parameters for the RSCE are given in Table 1.

Table 1. Hot press parameters for a 10-hour aerogel farication process. Courtesy S. Bakrania.[11]

step	temp (F)	rate (F/min)	load (kips)	load rate (lb/min)	dwell time (h:mm:ss)
1	440	1	17	600	0:00:30
2	560	10	17	600	0:15:30
3	440	10	2	600	0:00:30
4	90	2	1	600	0:00:30

Figure 6. Graphical representation of hot press temperature and pressure program. Courtesy S. Bakrania.[11]

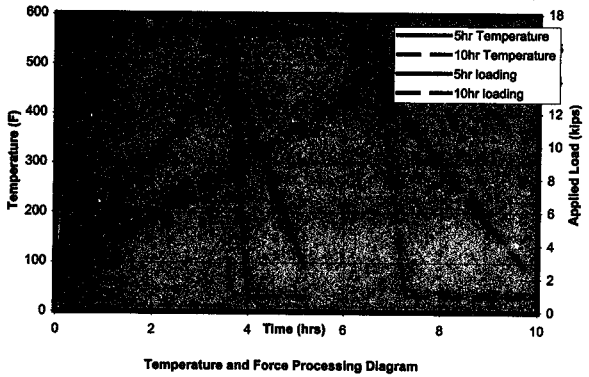

Excitation & emission spectra

A PTI Steady State Fluorometer System was utilized to obtain excitation and emission spectra of the solutions, xerogels, and aerogels. This system was comprised of a PTI A-1010 Arc Lamp, a PTI LPS-220B Lamp Power Supply, and a PTI Model 810/814 Photomultiplier Detection System. Samples were stored and analyzed in 10 x 10 x 45 mm polystyrene cuvettes. The parameters and slit widths for each measurement are listed in Table 2.

Table 2. Parameters used to collect steady-state fluorescence data in $Ru(dpp)_3^{2+}$ solutions, xerogels, and aerogels.

Sample (Figure #)	Excitation Slit Widths (nm)	Emission Slit Widths (nm)	Excitation Wavelength(s) (nm)	Emission Wavelength(s) (nm)
EtOH (10, 13)	2	4	350-525	615
EtOH (11,12, Xerogels (15)	2	4	464	500-800
EtOH (14)	2	4	464	500-875
Xerogels (16)	2	4	350-600	611
Aerogel (18)	4	4	446	500-750
Aerogel (19)	4	4	350-575	615

Time-based gas response measurements

The PTI Steady State Fluorometer System described above was used to determine the rate of response of $Ru(dpp)_3^{2+}$-doped and $Ru(bpy)_3^{2+}$-doped aerogels and xerogels to gaseous nitrogen ($N_2(g)$). The parameters used for data collection are given in Table 3. Sample cuvettes were uncapped and placed in the fluorometer. The $N_2(g)$ was impinged on the sample continuously or intermittently, depending on the experiment, as noted in the corresponding figures. Figure 7 depicts the gas inlet system. Note that the placement of the tygon tubing was modified for the solution trials to prevent sample evaporation.

Table 3. Parameters used to collect steady-state, time-based fluorescence data in $Ru(dpp)_3^{2+}$ solutions, xerogels, and aerogels.

Sample (Figure #)	Excitation Slit Widths (nm)	Emission Slit Widths (nm)	Excitation Wavelength(nm)	Emission Wavelength (nm)	Points/ s
EtOH (20)	2	2	446	615	2
Aerogel (21,22)	2	4	446	614	10
Xerogel (24)	1	1	446	613	2

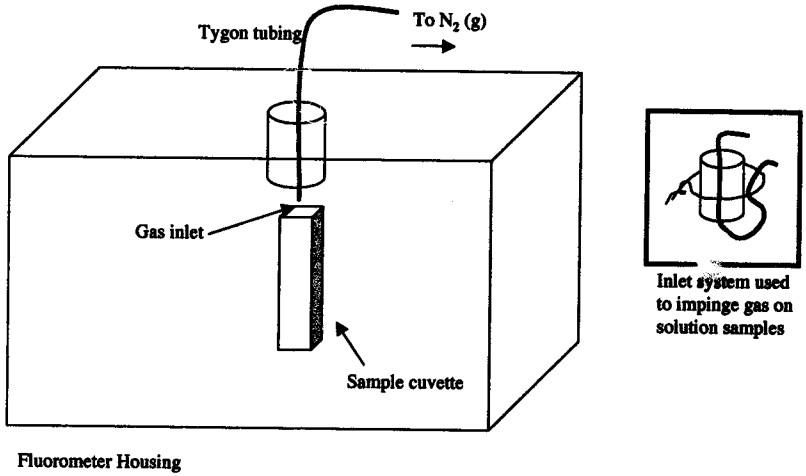

Figure 7. The gas flow system for time-based gas response analyses. For the aerogels, a flow rate of roughtly 1800 ml/min was used. For the xerogels, the flow rate was decreased, as higher flow rates caused the xerogel to move out of the excitation beam. For the solution, the inlet tubing was directed away from the sample (as shown in the inset), to deter solvent evaporation.

Gas response calibration curve measurements

The PTI Steady State Fluorometer System described above was used to calibrate the response of a $Ru(dpp)_3^{2+}$-doped aerogel to ambient oxygen concentration. All measurements were obtained at an excitation wavelength of 464 nm and an emission wavelength of 615 nm. The excitation slit widths were 2 nm, and the emission slit widths were 4 nm. The ambient oxygen content was controlled by mixing ultrapure air and N_2 (g) using a 150-mm Airgas Gas Proportioner. Gas proportioner settings are listed in Table 4. The second stage regulators were set to 20 psi for both N_2(g) and air. The line regulator was opened maximally and gave a reading of 17.5 psi. The flow rate into the cuvette was calculated to be 1800 ± 30 ml/min, using the manufacturer's calibration data for the gas proportioner. The gas mixing system is depicted in Figure 8. A cuvette cap was designed for direct delivery of the gas mixture to the sample and is depicted in Figure 8c.

Table 4. Gas proportioner settings used to develop the calibration curve. Gas proportions were set by adjusting level to the indicated reading. The proportioner calibration chart was used to determine the flow of each gas.

mix #	N_2(g) reading (mm)	N_2 flow (ml/min)	air reading (mm)	air flow (ml/min)	total flow (ml/min)	% air	% O_2
1	0	0	50	1801	1801	100	21.5
2	5	276	40	1497	1773	84.4	18.2
3	10	460	35	1335	1795	74.4	16.0
4	15	644	30	1172	1816	64.5	13.9
5	20	828	25	1000	1828	54.7	11.8
6	25	1000	20	828	1828	45.3	9.7
7	30	1172	15	644	1816	35.5	7.6
8	35	1335	10	460	1795	25.6	5.5
9	40	1497	5	276	1773	15.6	3.3
10	50	1801	0	0	1801	0	0

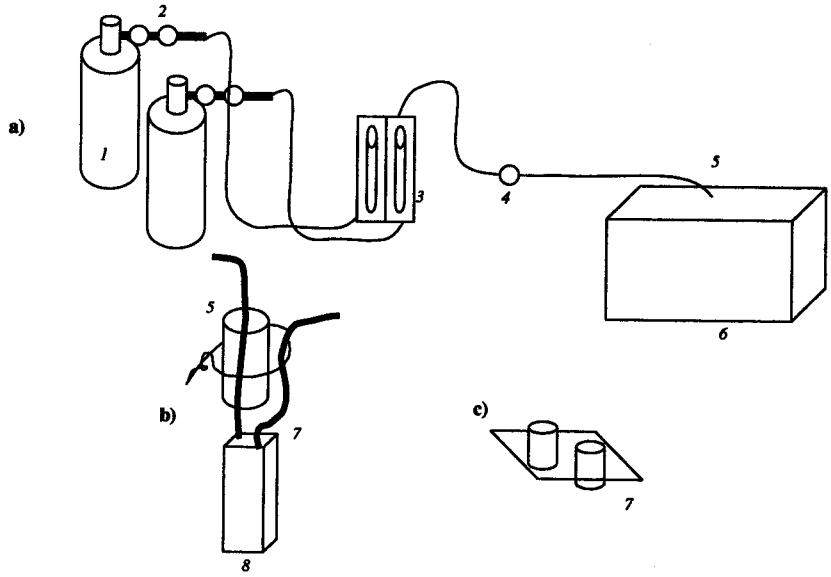

Figure 8. The gas mixing system. a) Gaseous nitrogen and ultrapure air *(1)* are delivered to tygon tubing via two-stage regulators *(2)*. The gasses are mixed in the gas proportioner *(3)*, then pass through a line regulator *(4)*, and through an injection port *(5)* to the fluorometer *(6)*. b) The gas mixture then flows through the inlet port (5) and the tubing is fed into the cuvette through a modified cuvette cap *(7)*. The sample is held in the cuvette *(8)*. The gas mixture is vented into the flurometer chamber through a piece of tygon *(9)*. c) Two holes were bored into the top of a cuvette cap *(7)*. The tygon tubing was threaded snugly through those holes.

Fluorescence lifetime decay measurements

A PTI Laser Strobe Fluorescence Lifetime System was used to measure the fluorescence lifetimes of the $Ru(dpp)_3^{2+}$ and $Ru(bpy)_3^{2+}$ in aerogels, xerogels, and in solution. Lifetime measurements were taken in both oxygen-rich (air) and oxygen-poor (positive pressure $N_2(g)$) environments. The instrument employs a pulsed nitrogen-pumped dye double laser. A PTI laser dye solution, PLD446 Coumarin 450, was used. All measurements were obtained using an excitation wavelength of 446nm, which is the maximum for the laser dye. All other parameters are listed in Table 5. A Ludox ® colloidal silica scatterer was used in conjunction with a Thermo Oriel 50540 filter for all systems that exhibited short lifetimes (i.e. doped aerogels in air).

Table 5. Parameters used to collect fluorescence lifetime data. a) $Ru(dpp)_3^{2+}$-doped aerogels, **b)** $Ru(bpy)_3^{2+}$-doped aerogels, **c)** $Ru(bpy)_3^{2+}$-doped xerogels, **d)** $Ru(bpy)_3^{2+}$-doped xerogels, **e)** $Ru(dpp)_3^{2+}$ solution in $N_2(g)$. Aerogels and xerogels were deaerated by continuous flow of $N_2(g)$ directly over the sample, as depicted in Figure 7. For the $Ru(dpp)_3^{2+}$ solution in $N_2(g)$, the fluorometer chamber was flooded with $N_2(g)$ for more than 70 min. All aerogel samples were run with a scatterer, λ_{ex}= 446nm. An asterix (*) indicates that $\lambda_{, scatterer}$ =449 nm.

a) $Ru(dpp)_3^{2+}$-doped aerogels

Gaseous Environment	Component (s)	Slits (nm)	λ_{em} (nm)	Delay (ns)	Channels	Averages
air	τ_1	4	615	40-240	200	5
air	τ_2	4	615	40-2040	200	5
N_2	τ_1	10	615	200-9200	900	15
N_2	$\tau_1 + \tau_2$	5	615*	45-105	120	10

b) $Ru(bpy)_3^{2+}$-doped aerogels

Gaseous Environment	Component (s)	Slits (nm)	λ_{em} (nm)	Delay (ns)	Channels	Averages
air	τ_2	8	590*	40-2040	200	10
air	$\tau_1 + \tau_2$	8	590*	40-2040	200	10
N_2	τ_1	6	615*	40-240	200	10
N_2	τ_2	10	615	200-9200	900	15

c) $Ru(dpp)_3^{2+}$-doped xerogels

Gaseous Environment	Component (s)	Slits (nm)	λ_{em} (nm)	Delay (ns)	Channels	Averages
air	$\tau_1 + \tau_2$	12	613	35-4035	200	15
N_2	$\tau_1 + \tau_2$	10	615	40-9040	900	15

d) $Ru(bpy)_3^{2+}$-doped xerogels

Gaseous Environment	Component (s)	Slits (nm)	λ_{em} (nm)	Delay (ns)	Channels	Averages
air	$\tau_1 + \tau_2$	8	590	40-9040	900	15
N_2	$\tau_1 + \tau_2$	8	590	40-9040	900	15

e) $Ru(bpy)_3^{2+}$ in EtOH solution

N_2	τ_1	6	615	40-9040	900	3

Results & Discussion

I. Fluorescence Spectral Properties of $Ru(dpp)_3^{2+}$/EtOH Solutions

In an ethanol solution, the absorption spectrum of $Ru(dpp)_3^{2+}$ changes in both shape and intensity with respect to fluorophore concentration, as shown in Figure 9a. The most concentrated solution, 1.0×10^{-3} M, absorbs strongly from around 325 to 560 nm. Since most of the incident light is absorbed by the sample, few photons are transmitted to the detector, greatly decreasing the signal-to-noise ratio. The spectrum of the 1.0×10^{-4} M solution has a broad peak from 420 to 480 nm. The most dilute solution, 1.0×10^{-5} M, has absorbances within the response range of the instrument, and the shape of the spectrum was very similar to that of the 1.0×10^{-4} M solution. The absorption spectrum of a saturated aqueous solution of $Ru(dpp)_3^{2+}$ is nearly identical in shape to the 1.0×10^{-4} M $Ru(dpp)_3^{2+}$/EtOH solution spectrum.

Each of the $Ru(dpp)_3^{2+}$ solutions had a different color, as pictured in Figure 9b. The most concentrated solution, 1.0×10^{-3} M, was a vibrant red-orange, the 1.0×10^{-4} M solution was orange, and the 1.0×10^{-5} M solution was a pale yellow. One normally expects that variable concentrations of the same solution will vary in shade, but not color. Their absorption spectra are expected to share the same shape, while varying in intensity. Different absorption spectra indicate the existence of different chemical species in the solution, and we therefore suspect that aggregates of $Ru(dpp)_3^{2+}$ form at higher concentrations. The formation of this different species would account for the change in spectral shape, and hence the observable differences in solution color.

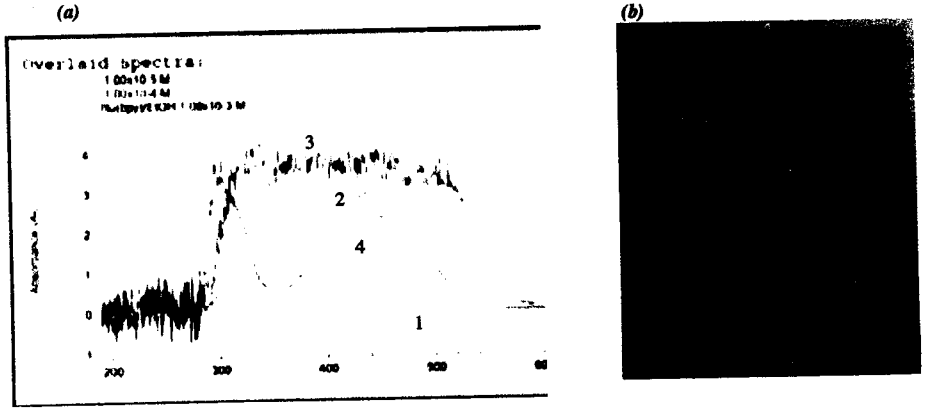

Figure 9. $Ru(dpp)_3^{2+}$ solutions. (a) Absorption spectra of four solutions: (1) 1.0×10^{-5} M $Ru(dpp)_3^{2+}$ in EtOH, (2) 1.0×10^{-4} M $Ru(dpp)_3^{2+}$ in EtOH, (3) 1.0×10^{-3} M $Ru(dpp)_3^{2+}$ in EtOH, and (4) a water saturated $Ru(dpp)_3^{2+}$ in water solution. These spectra were collected using an HP 8453a UV-Visible Diode Array Spectrophotometer. (b) Digital photo of $Ru(dpp)_3^{2+}$ solutions. between the solutions. The most dilute solution (1) is yellow, a more concentrated solution (2) is orange, and the most concentrated solution (3) is red-orange.

The excitation spectra of these $Ru(dpp)_3^{2+}$ /EtOH solutions is shown in Figure 10. The spectrum of the 1.0×10^{-5} M solution agrees with the absorption spectrum shown in Figure 9a. At higher concentrations, 1.0×10^{-4} M and 1.0×10^{-3} M $Ru(dpp)_3^{2+}$, there is a dramatic change in the shape of the excitation spectrum. The 1.0×10^{-4} M solution has a broad drop in fluorescence intensity when excited from roughly 395 to 490 nm, with peaks at 372 and 510 nm. The 1.0×10^{-5} M solution exhibits very low fluorescence intensity when excited by light from 360 to 520 nm. The drop in fluorescence emission intensity in the more concentrated samples could be due to a strong absorbance at these wavelengths, or result from the failure of the excitation light to travel through the whole sample. As the absorbance is so high for the more concentrated samples, it is difficult to assess whether or not aggregation is occurring at higher $Ru(dpp)_3^{2+}$ concentrations.

The emission spectra of these $Ru(dpp)_3^{2+}$ /EtOH solutions is shown in Figure 11. The spectra of the 1.0×10^{-3} M, 1.0×10^{-4} M and 1.0×10^{-5} M solutions have peaks in emission intensity at 618, 617, and 616 nm, respectively. These shifts are not significantly different, as the emission slit were 4 nm wide (Table 2). The latter two solutions share the same spectral shape, while the most concentrated solution has a broad shoulder from roughly 655 to 740 nm. Clearly, the character of the fluorophore changes once the $Ru(dpp)_3^{2+}$ concentration is above some critical point. Hara *et al.*[16] suspect that ruthenium(II) bis(4,7-diphenyl-1,10-phenanthroline) and modified ruthenium (II) tris (1,10-phenanthroline) complexes aggregate in TiO_2 nanocrystalline structures, and it is possible that we are observing the effects of such aggregation in solution.

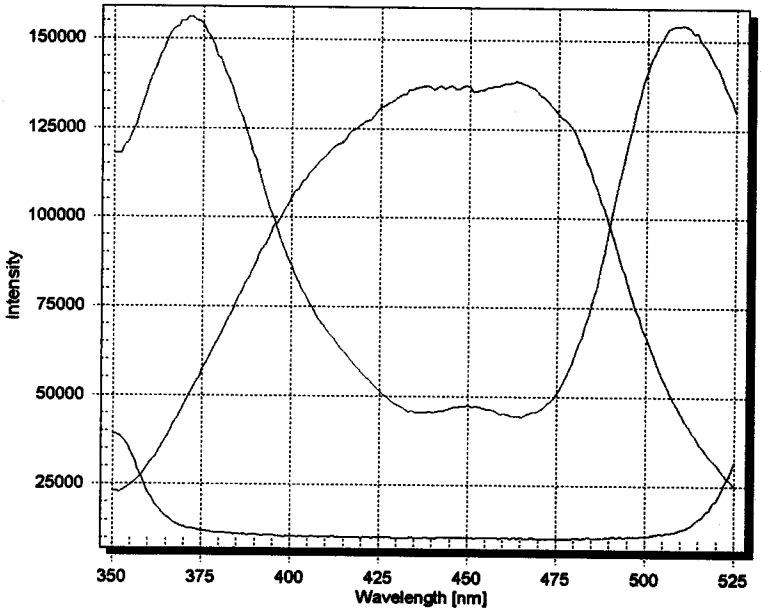

Figure 10. Corrected excitation spectra of three more concentrated $[Ru(dpp)_3]^{2+}$ in absolute EtOH. The most concentrated solution, 1.0 x 10^{-3} M, is shown in royal blue. The 1.0 x 10^{-4} M solution is shown in green, and the 1.0 x 10^{-5} M is shown in red. The drop in fluorescence intensity in the more concentrated samples could be due to a strong absorbance at these wavelengths, or result from the failure of the excitation light to travel through the whole sample. Ex slits = 2 nm, Em slits = 4 nm, λ_{em} = 615 nm.

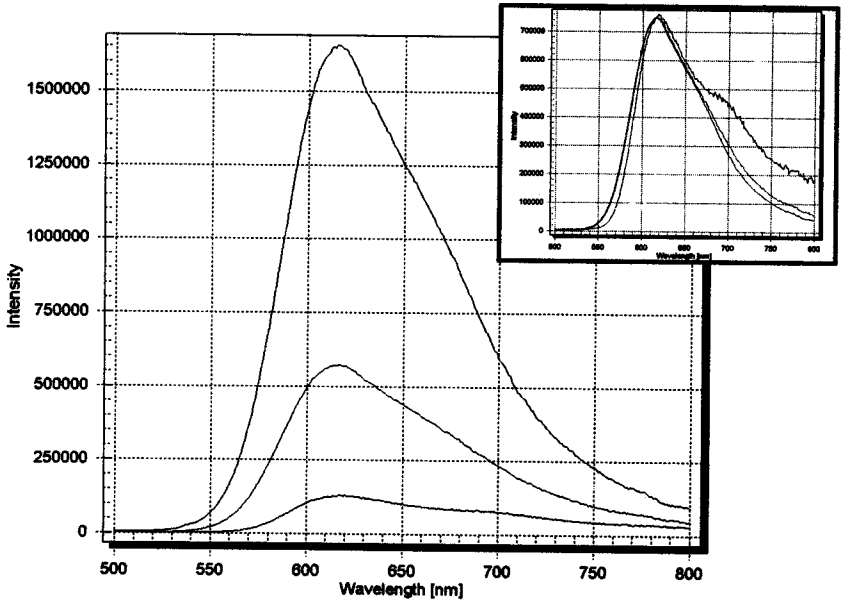

Figure 11. Corrected emission spectra of $[Ru(dpp)_3]^{2+}$ in absolute EtOH. The most concentrated solution, 1.0×10^{-3} M, is shown in royal blue. The 1.0×10^{-4} M solution is shown in green,and the 1.0×10^{-5} M is shown in red. For the 1.0×10^{-3} M solution, $\lambda_{max} = 618$ nm; for the 1.0×10^{-4} M solution, $\lambda_{max} = 617$ nm; and for the 1.0×10^{-5} M solution, $\lambda_{max} = 616$ nm. These emission maxima are not significantly different. The most concentrated solution has a broad shoulder from 655 to 740 nm, as seen in the inset, which shows the normalized data. Ex slits = 2 nm, Em slits = 4 nm, $\lambda_{ex} = 464$ nm.

To test the linearity of the fluorescence with respect to concentration, six $Ru(dpp)_3^{2+}$ solutions were prepared, with concentrations ranging from 2.5×10^{-7} M to 1.0×10^{-5} M. The shapes of the emission spectra of the 2.5×10^{-7} M to 5.0×10^{-6} M $Ru(dpp)_3^{2+}$ solutions are consistent, with peaks at 537 and 615nm, as indicated in Figure 12. At higher concentrations, 1.0×10^{-5} and 5.0×10^{-6} M $Ru(dpp)_3^{2+}$, the peak at 537 nm is less prominent, as it is being masked by the peak at 615 nm. We believe that this peak at 537 nm is due to scatter. The peak at 615 nm has a shoulder from around 630 nm to 660 nm. The presence of multiple fluorescence bands usually indicates that the fluorescence is occurring from separate chemical species[13], and this shoulder may be arising from the formation of another fluorescent species, such as a $Ru(dpp)_3^{2+}$ aggregation complex.

The fluorescence intensity at 537 nm varies linearly with respect to $Ru(dpp)_3^{2+}$ concentration from 1.0×10^{-6} M to 1.0×10^{-5} M. A plot of the data gave a line described by $I = (3.2 \times 10^{9})C + 3.7 \times 10^{4}$ with an R^2 value of 0.994, where I is the fluorescence intensity and C is the molar concentration of the sample. The intensity at 615 nm varies linearly from 5.0×10^{-7} M to 5.0×10^{-6} M, where the equation of the line was $I = (5.7 \times 10^{11})C + 1.2 \times 10^{5}$ with an R^2 value of 0.995.

Figure 13 shows that the shape of the excitation spectra of the 2.5×10^{-7} M to 1.0×10^{-5} M $Ru(dpp)_3^{2+}$ solutions are consistent. There is a broad, double-humped peak ranging from roughly 425 to 475 nm, with peaks at 437 and 463 nm. This has the same shape as the absorption spectrum of a 1.0×10^{-5} M $Ru(dpp)_3^{2+}$ solution; there is no evidence of

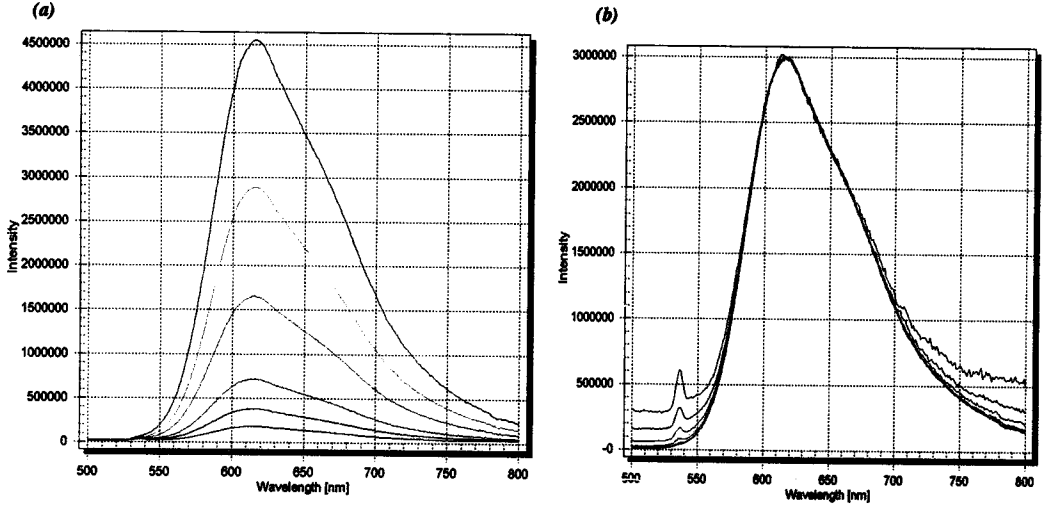

Figure 12. ***(a)*** **Corrected emission spectra of six $[Ru(dpp)_3]^{2+}$ in standard grade EtOH.** The most concentrated solution, 1.0×10^{-5} M, is shown in red. The 5.0×10^{-6} M solution is shown in orange, 2.5×10^{-6} M: bright green, 1.0×10^{-6} M: cobalt blue, 5.0×10^{-7} M: royal blue, 2.5×10^{-7} M: violet. For all solutions $\lambda_{max1} = 615$ nm and $\lambda_{max2} = 537$ nm, except for the 2.5×10^{-7}M and 5.0×10^{-7} M solutions, which had $\lambda_{max2} = 536$ nm. An enlarged view of the broad peak at 537 nm is shown in the inset. ***(b)*** **Normalized emission spectra.** The peak at 615 nm in (a) was normalized to an intensity of 3000000. All solutions are represented using the same color scheme as in (a). Ex slits = 2 nm, Em slits = 4 nm, $\lambda_{ex} = 464$ nm.

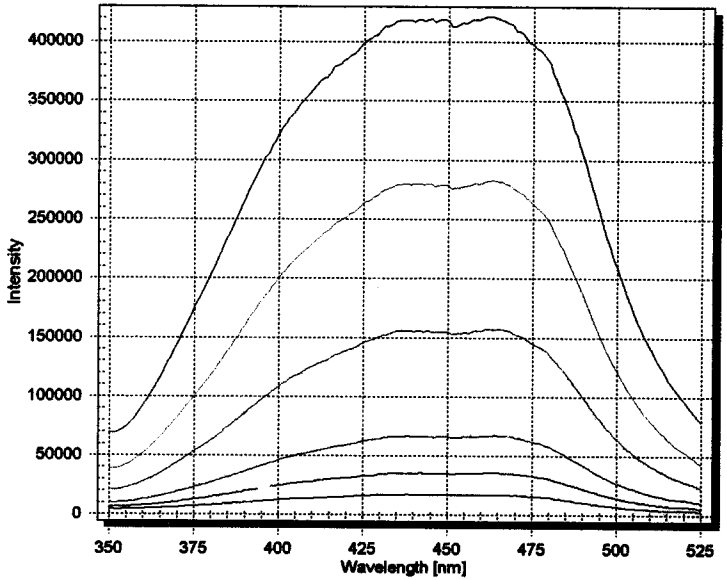

Figure 13. Corrected excitation spectra of six $[Ru(dpp)_3]^{2+}$ in standard grade EtOH. The most concentrated solution, 1.0×10^{-5} M, is shown in red. The 5.0×10^{-6} M solution is shown in orange, 2.5×10^{-6} M: bright green, 1.0×10^{-6} M: cobalt blue, 5.0×10^{-7} M: royal blue, 2.5×10^{-7} M: violet. For all solutions $\lambda_{max1} = 437$ nm and $\lambda_{max2} = 463$ nm. Ex slits = 2 nm, Em slits = 4 nm, $\lambda_{em} = 615$ nm.

aggregation at these concentrations. This excitation spectrum is not a mirror image of the emission spectrum, indicating that the vibrational spacings are different in the ground and excited states[9]. The fluorescence intensity at 437 nm varies linearly from 2.5×10^{-7} M to 5.0×10^{-6} M $Ru(dpp)_3^{2+}$: $I=(5.5 \times 10^{10})C + 9.0 \times 10^3$ with an R^2 value of 0.997. The intensity at 463 nm also varies linearly from 2.5×10^{-7} M to 5.0×10^{-6} M $Ru(dpp)_3^{2+}$: $I=(5.6 \times 10^{10})C + 9.1 \times 10^3$ with an R^2 value of 0.997.

To test the effect of oxygen on a $Ru(dpp)_3^{2+}$ solution, emission spectra were obtained of the solution in air and in nitrogen. As shown in Figure 14, the 5.0×10^{-6} M $Ru(dpp)_3^{2+}$ solution exhibited a 6.3-fold increase in fluorescence intensity after it was vigorously bubbled with $N_2(g)$. The dramatic increase in fluorescence intensity coincident with the removal of ambient $O_2(g)$ indicates that $O_2(g)$ quenches $Ru(dpp)_3^{2+}$ fluorescence, as previously demonstrated by Carraway *et al.*[17] This oxygen sensitivity makes $Ru(dpp)_3^{2+}$ an attractive probe for use as a gas sensor in an aerogel platform. (Note that during the emission scan of the deaerated sample, oxygen diffused into the doped aerogel).

The peak of the emission spectrum red-shifted from 615 to 619 nm when going from an oxygen-rich (20.8 % O_2 in air) to an oxygen-poor (N_2 bubbled) sample. This shift is significant, as the emission slit widths were set to 4 nm.

The fluorescence lifetime of a deaerated 1.0×10^{-5} M $Ru(dpp)_3^{2+}$/EtOH solution was found to be $(464 \pm 3) \times 10^1$ ns ($\chi^2 = 1.036$), which agrees respectably (5.0% error) with that reported by Mongey et. al. for $Ru(dpp)_3^{2+}$ in a 4:1 EtOH/H_20 solution (4890 ns).[18]

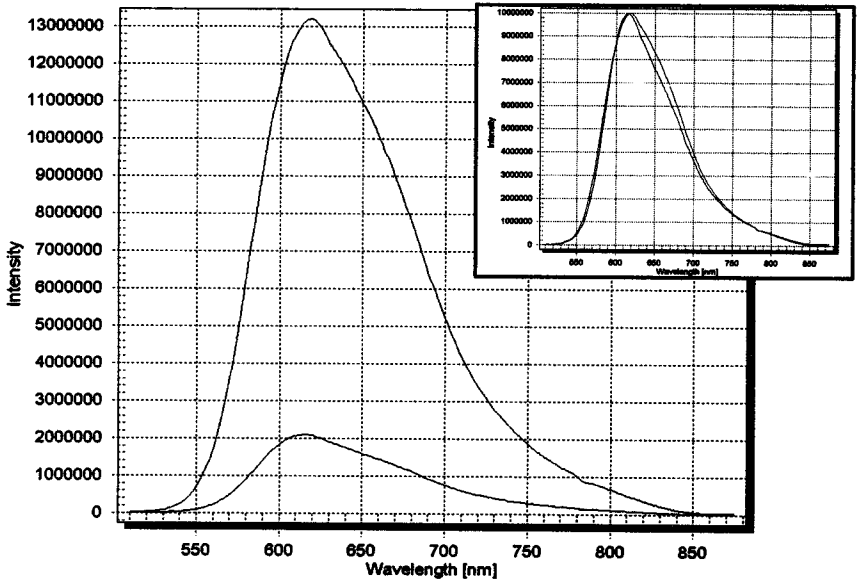

Figure 14. Corrected emission spectra of $Ru(dpp)_3^{2+}$ in EtOH solution in air and in N_2(g). A 5.0 x 10^{-6} M $Ru(dpp)_3^{2+}$ solution was deaerated by vigorous bubbling with N_2(g) for 8 minutes. The spectrum of the deaerated solution is shown in red. The sample was then reaerated by bubbling with air for 8 minutes. The spectrum of the aerated solution is shown in blue. The inset shows the normalized spectra: λ_{max}= 619 nm in the deaerated sample, λ_{max} = 615 nm in the oxygen-rich sample. Note that during the emission scan of the deaerated sample, oxygen diffused into the sample. Ex slits = 2 nm, Em slits = 4 nm, λ_{ex} = 464 nm.

II. Fluorescence Spectral Properties of $Ru(dpp)_3^{2+}$- doped Xerogels

Three different concentrations of $Ru(dpp)_3^{2+}$/ EtOH were successfully doped into xerogels, and the emission spectra of those gels are shown in Figure 15. All of the spectra are blue shifted relative to the solution samples, with peaks at 602, 609, and 611 nm for xerogels prepared with 1.0×10^{-5} M, 1.0×10^{-4} M, and 1.0×10^{-3} M $Ru(dpp)_3^{2+}$ solutions, respectively. The shift in peak emission wavelength indicates that the character of the fluorophore is different in each of the xerogels. That is, the environment of the complex varies with respect to $Ru(dpp)_3^{2+}$ concentration. The complexes in xerogels prepared from a lower-concentration $Ru(dpp)_3^{2+}$ solution are in higher energy environments (blue-shifted) than their more concentrated analogs. This indicates that either (1) the character of the probe or (2) the probe micro-environments within the sol-gel matrix varies with changes in fluorophore concentration. Presumably, movement into a more constrained environment of the matrix (i.e. the pore-matrix interface) would increase the energy of the fluorophore complex, thereby blue-shifting the emission spectra. In the more concentrated xerogels, the fluorophore could be partitioning both to the silica surface as well as into the pore space. The increased motion of the population of $Ru(dpp)_3^{2+}$ moieties that exist in the pore space would red-shift the emission spectrum. A red-shifted spectrum could also be the result of $Ru(dpp)_3^{2+}$ aggregation at higher concentration, which may decrease the overall energy of the electronic transition by giving the complex a more aromatic-like character.

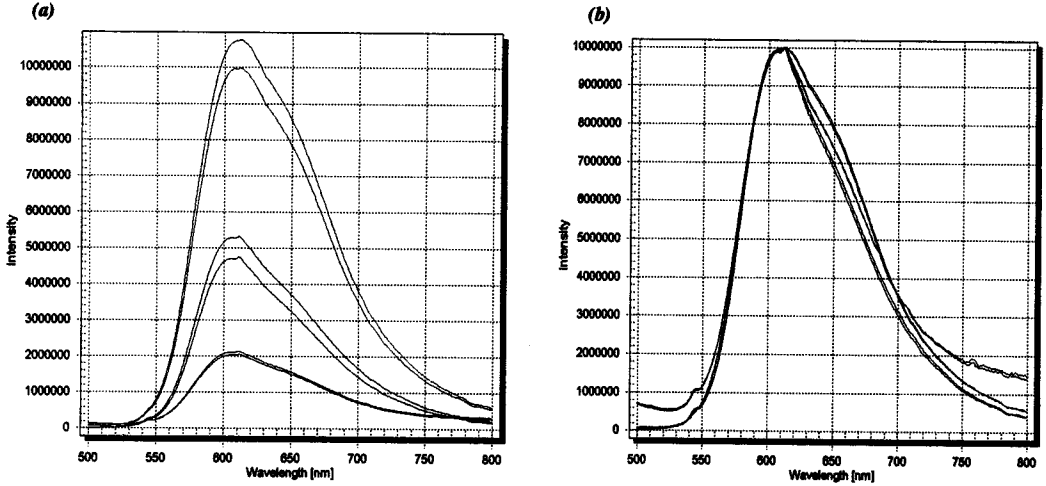

Figure 15. ***(a)*** **Corrected emission spectra of $[Ru(dpp)_3]^{2+}$ -doped xerogels.** Spectra of two xerogels prepared from a 1.0×10^{-3} M $[Ru(dpp)_3]^{2+}$ solution are shown in royal blue. The 1.0×10^{-4} M -doped xerogels are shown in green, and the 1.0×10^{-5} M- doped xerogels are shown in red. ***(b)*** **Normalized emission spectra.** For the 1.0×10^{-3} M - doped xerogel, $\lambda_{max} = 611$nm; for the 1.0×10^{-4} M -doped xerogel, $\lambda_{max} = 609$ nm; and for the 1.0×10^{-5} M-doped xerogel, $\lambda_{max} = 602$ nm. Ex slits = 2 nm, Em slits = 4 nm, $\lambda_{ex} = 464$ nm.

Indeed, when the spectra are normalized (Figure 15 b), it is clear that samples prepared from different $Ru(dpp)_3^{2+}$ concentrations do not have the same emission spectrum shape. The xerogel prepared from 1.0×10^{-4} M $Ru(dpp)_3^{2+}$ has a shoulder around 640 nm, and the xerogel prepared from 1.0×10^{-5} M $Ru(dpp)_3^{2+}$ has a broader peak than those of the 1.0×10^{-4} M $Ru(dpp)_3^{2+}$ and 1.0×10^{-3} M $Ru(dpp)_3^{2+}$ prepared xerogels. Again, this broader peak could be the result of the probe molecule existing in several micro-environments. The dependence on the fluorescence lifetime decay (both the number of lifetimes as well as the rate of decay) on the $Ru(dpp)_3^{2+}$ concentration could help determine if the probe is portioning into several different environments within the xerogels. The most intense fluorescence was observed in the xerogel prepared from 1.0×10^{-4} M $Ru(dpp)_3^{2+}$ solution, and not the xerogel prepared from 1.0×10^{-3} M $Ru(dpp)_3^{2+}$ solution, as one may expect due to the higher fluorophore concentration in the latter. This could result from failure of the light source to travel through the entire length of the xerogel, limiting fluorescence from the xerogel's center, or limited absorbance at the excitation wavelenth (464 nm). It could also be the result of self-quenching, which is likely to occur during fluorophore aggregation.

The excitation spectra of these xerogels are shown in Figure 16. The excitation spectra of the 1.0×10^{-5} M $Ru(dpp)_3^{2+}$ and 1.0×10^{-4} M $Ru(dpp)_3^{2+}$ samples were very similar to one another, with a broad distinct peak from 425 to 475 nm. The shape of the 1.0×10^{-3} M $Ru(dpp)_3^{2+}$ xerogel spectrum was notably different, exhibiting limited intensity when excited from 425-475 nm and peaks at 372 nm and 514 nm. It is worthy of note that in the xerogel prepared from 1.0×10^{-3} M $Ru(dpp)_3^{2+}$, we observed that the incident light

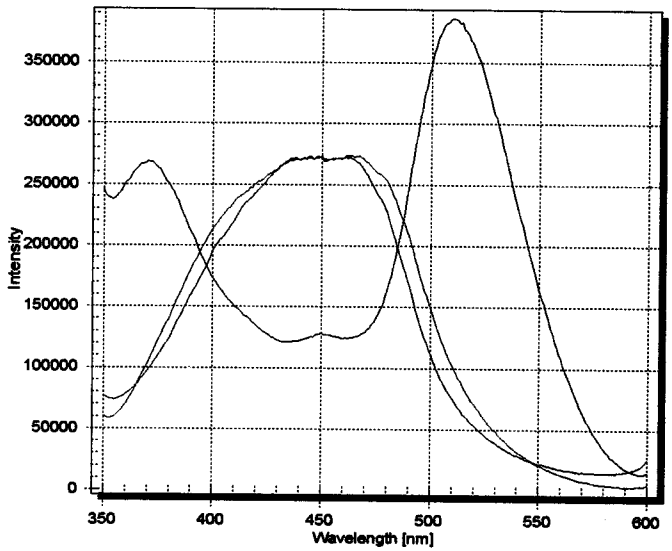

Figure 16. Corrected excitation spectra of $[Ru(dpp)_3]^{2+}$ -doped xerogels. The xerogels prepared from a 1.0×10^{-3} M $[Ru(dpp)_3]^{2+}$ solution are shown in royal blue. The 1.0×10^{-4} M -doped xerogel is shown in green,and the 1.0×10^{-5} M- doped xerogel is shown in red. For the 1.0×10^{-5} M and 1.0×10^{-4} M - doped xerogels, there is a broad peak from around 425 to 475 nm. The 1.0×10^{-3} M -doped xerogel exhibited limited intensity over this range, and had $\lambda_{max1} = 372$ nm and $\lambda_{max2} = 514$ nm. This is likely due to the strong absorption of the more concentrated sample. Ex slits = 2 nm, Em slits = 4 nm, $\lambda_{em} = 611$ nm.

was not traveling through the entire sample, as depicted in Figure 17. When the light cannot reach the sample interior, only a small population of probes can be excited in that portion of the sample from which fluorescence intensity is collected, resulting in a decrease in observed excitation intensity. Recall that the emission scan of this sample (1.0×10^{-3} M $Ru(dpp)_3^{2+}$-doped xerogel) had limited fluorescence intensity at 615 nm. This is likely a direct result of the limited excitation of the probed sample. The distinct and unusual difference in spectral properties of the xerogel prepared with different $Ru(dpp)_3^{2+}$ solution concentrations indicates a clear change in the fluorphore environment and behavior in the xerogels prepared with higher concentrations of $Ru(dpp)_3^{2+}$.

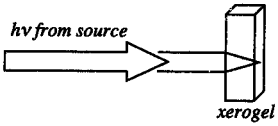

Figure 17. Diagram of cone-shape formed by the incident light with 1.0×10^{-3} M $Ru(dpp)_3^{2+}$ -doped xerogel.

III. $Ru(dpp)_3^{2+}$- doped Aerogels: Fluorescence Spectral Properties

Two different concentrations of $Ru(dpp)_3^{2+}$/ EtOH, 1.0×10^{-5} M and 1.0×10^{-4} M, were successfully doped into aerogel matrices. Six aerogel samples of each concentration were prepared simultaneously, and the emission spectra of the replicates agreed respectably with one exception. One aerogel prepared with 1.0×10^{-5} M $Ru(dpp)_3^{2+}$ had a notably different spectrum from the others. Representative emission spectra of the 1.0×10^{-5} M $Ru(dpp)_3^{2+}$ and 1.0×10^{-4} M $Ru(dpp)_3^{2+}$ aerogels are shown in Figure 18a

Figure 18b, respectively. The emission spectrum of the aerogel prepared from 1.0×10^{-5} M $Ru(dpp)_3^{2+}$ solution had a peak at 602 nm, blue-shifted relative to the 615-nm peak of the solution samples. This is consistent with the corresponding 1.0×10^{-5} M $Ru(dpp)_3^{2+}$-doped xerogel, which had an emission peak at 602 nm. Hence, the $Ru(dpp)_3^{2+}$ probe has higher energy spacings in the aerogel environment as compared to the EtOH solution environment, whereas the environment of the probe in the xerogel and the aerogel is very similar for these samples. Solvent effects of the EtOH, which can hydrogen bond to the lone pairs on the phenanthroline nitrogens, may contribute to this difference in fluorophore energy spacing. The rotational motion of $Ru(dpp)_3^{2+}$ is anticipated to be much less constrained in solution, giving the probe lower energy and a red-shifted spectrum relative to the more constrained environment of the aerogel. There are three other signals, at 577, 660, and 681nm, that appear to be due to scattering.

Figure 18b shows the emission spectrum of the aerogel prepared from 1.0×10^{-4} M $Ru(dpp)_3^{2+}$, which clearly has a different spectral shape than the aerogel prepared from 1.0×10^{-5} M $Ru(dpp)_3^{2+}$ solution. The latter has a broad peak at 616 nm and much less scattering and noise when compared to the former, which had a peak at 602 nm. This red-shift in the more concentrated aerogel could be due to increased probe-probe interactions. The presence of solvent would interfere with probe-probe interactions, thereby limiting the extent of the red shift. Hence, one would expect the fluorescence of $Ru(dpp)_3^{2+}$ in a wet xerogel to be less red-shifted than if it were in an aerogel, giving the doped xerogel a lower emission maximum. Indeed, the 1.0×10^{-4} M $Ru(dpp)_3^{2+}$-doped

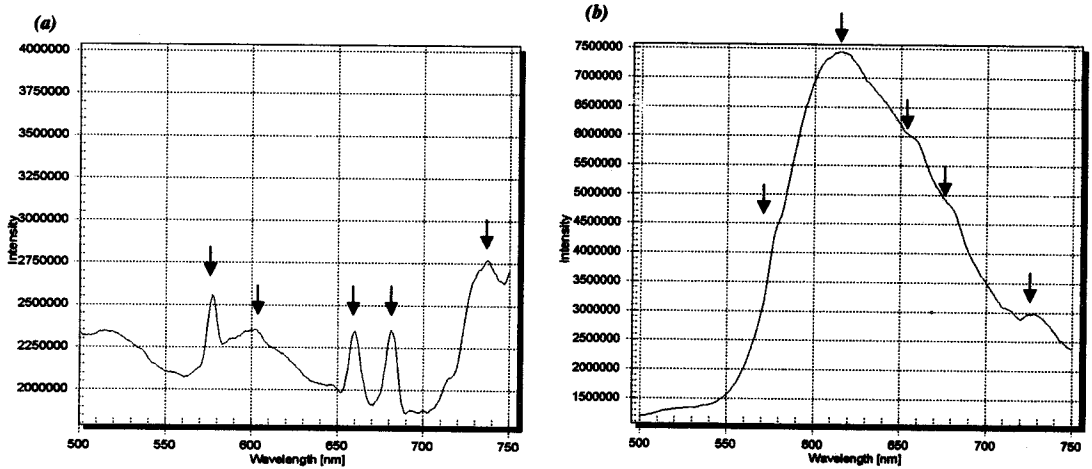

Figure 18. Corrected emission spectra of $[Ru(dpp)_3]^{2+}$ -doped aerogels. *(a)* An aerogel prepared from a 1.0×10^{-5} M $[Ru(dpp)_3]^{2+}$ solution, shown in red, $\lambda_{max} = 602$ nm . The peaks at 578, 660, and 682 nm appear to be due to scatter. These scattering peaks are also present in (b). Note the corresponding spectral features, which are marked with arrows. *(b)* An aerogel prepared from a 1.0×10^{-4} M $[Ru(dpp)_3]^{2+}$ solution, shown in green, $\lambda_{max} = 616$ nm. Ex slits = 2 nm, Em slits = 4 nm, $\lambda_{ex} = 446$ nm.

aerogel had a higher emission maximum (616 nm) than a xerogel prepared from the same solution, which had a peak in emission at 609 nm.

There was a considerable amount of noise and scatter in the excitation spectra of the 1.0×10^{-5} M $Ru(dpp)_3^{2+}$-doped aerogel samples, which had consistent spectral shape for all but one of the samples (Figure 19a). The 1.0×10^{-4} M $Ru(dpp)_3^{2+}$-doped aerogel samples also agreed well, and a representative excitation spectrum is shown in Figure 19b. There was a broad, flat peak from 375 to 475 nm in the 1.0×10^{-5} M $Ru(dpp)_3^{2+}$-doped sample, whereas there was a broad peak at 457 nm in the 1.0×10^{-4} M $Ru(dpp)_3^{2+}$-doped sample. The range of both peaks is consistent with absorbance of the $Ru(dpp)_3^{2+}$ solutions, although the peak is more pronounced in the 1.0×10^{-4} M $Ru(dpp)_3^{2+}$-doped aerogels.

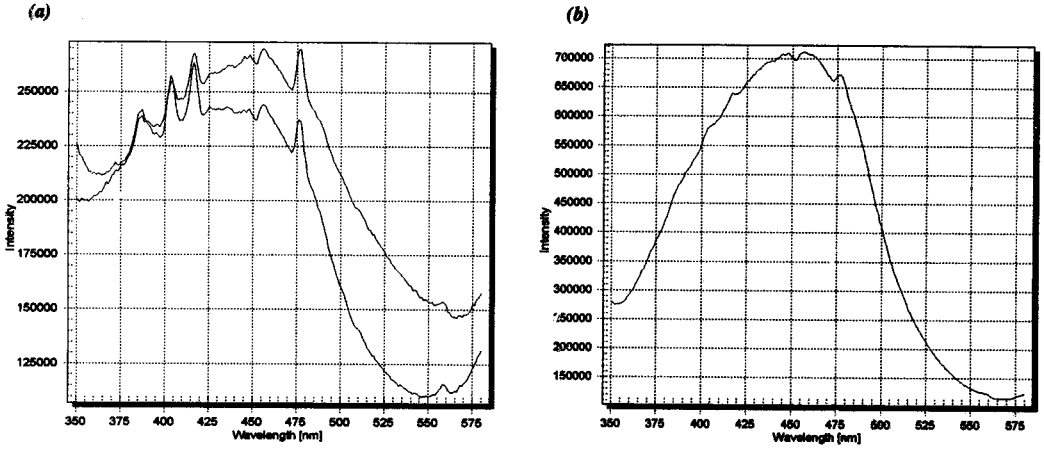

Figure 19. Corrected excitation spectra of $[Ru(dpp)_3]^{2+}$-doped aerogels. *(a)* An aerogel prepared from a 1.0×10^{-5} M $[Ru(dpp)_3]^{2+}$ solution, shown in red, gave a broad peak from 375 to 475 nm. A replicate of this aerogel, prepared in the same batch, gave a slightly different spectrum, shown in violet. The peaks at 387, 403, 416, 456, and 476 nm, appear to be scattering peaks. *(b)* An aerogel prepared from a 1.0×10^{-4} M $[Ru(dpp)_3]^{2+}$ solution, shown in green, gave a broad peak with $\lambda_{max} = 457$ nm. Ex slits = 2 nm, Em slits = 4 nm, $\lambda_{em} = 615$ nm.

IV. $Ru(dpp)_3^{2+}$ & $Ru(bpy)_3^{2+}$-doped Aerogels: Fluorescence Lifetime Dependence on Ambient O_2 (g) Concentration

The aerogel doped with 1.0×10^{-4} M $Ru(dpp)_3^{2+}$ solution exhibited two lifetimes in air: $\tau_1 = 2.117 \pm 0.044$ ns ($\chi^2 = 0.98$) and $\tau_2 = 562 \pm 37$ ns ($\chi^2 = 1.001$). These results are summarized in Table 6. The existence of two decay pathways indicates that the $Ru(dpp)_3^{2+}$ probe is proportioning into two micro-environments within the aerogel matrix. The shorter lifetime, τ_1, likely represents the fluorescence decay of the fluorophore in a constrained environment. In such an environment, there is a larger population of adjacent molecules in close proximity to the $Ru(dpp)_3^{2+}$ complex, and collisional interactions with those molecules offer additional pathways for fluorescence decay, thereby decreasing the lifetime of the fluorophore. The second decay pathway, τ_2, was much longer, indicating that the $Ru(dpp)_3^{2+}$ molecules might be in a less constrained environment.

Table 6. Fluorescence lifetime of $Ru(dpp)_3^{2+}$ and $Ru(bpy)_3^{2+}$- doped aerogels in the presence and absence of O_2(g).

	$Ru(dpp)_3^{2+}$ -doped aerogel		$Ru(bpy)_3^{2+}$ - doped aerogel	
	Air	Nitrogen	Air	Nitrogen
τ_1 (ns)	2.117 ± 0.044	4.601 ± 0.018	4.65 ± 0.24	4.68 ± 0.31
χ^2	0.98	1.011	0.9813	1.033
τ_2 (ns)	562 ± 37	4851 ± 53	771 ± 17	1583 ± 11
χ^2	1.001	1.011	1.016	1.082

In N_2(g), the $Ru(dpp)_3^{2+}$-doped aerogel exhibited much longer decay lifetimes where $\tau_1 = 4.601 \pm 0.018$ ns ($\chi^2 = 1.011$) and $\tau_2 = 4851 \pm 53$ ns ($\chi^2 = 1.011$). The lifetime from the constrained fluorophore environment, τ_1, was affected by the presence of oxygen to a much lesser extent than the lifetime arising from the less constrained environment, τ_2.

The fluorescence of a chemical species is dependent on the concentration of fluorescence quencher, which was uniform in these samples throughout the measurements. Clearly, the access of the $Ru(dpp)_3^{2+}$ probe to oxygen is different in the two micro-environments. In the more constrained environment (τ_1), there is limited fluid access to the probe, thereby limiting the effect of oxygen concentration on the fluorescence decay of the fluorophore. In the less constrained environment (τ_2), the fluid has open access to the probe molecules, so the composition of the fluid greatly affects the fluorescence decay of the probe. Presumably, the $Ru(dpp)_3^{2+}$ molecule is partitioning into the pore space (less constrained environment, τ_1), adhering to the silica matrix surface through charge-charge interactions, as well as into the interior of the silica matrix itself (constrained environment, τ_1).

This portioning into separate microenvironments is also evident in aerogels doped with 1.0×10^{-4} M $Ru(bpy)_3^{2+}$ solutions. These $Ru(bpy)_3^{2+}$-doped aerogels exhibited two distinct lifetimes in air, where $\tau_1 = 4.65 \pm 0.24$ ns ($\chi^2 = 0.9813$) and $\tau_2 = 771 \pm 17$ ns ($\chi^2 = 1.016$). These results are summarized in Table 6. In N_2(g), the $Ru(bpy)_3^{2+}$-doped aerogel exhibited longer decay lifetimes: $\tau_1 = 4.68 \pm 0.31$ ns ($\chi^2 = 1.033$) and $\tau_2 = 1583 \pm 11$ns ($\chi^2 = 1.082$). As was the case for the $Ru(dpp)_3^{2+}$-doped aerogels, the effect of oxygen quenching was more pronounced in the less-constrained (τ_2) microenvironment, again indicating that fluids have limited access to the more-constrained environment.

V. $Ru(dpp)_3^{2+}$ & $Ru(bpy)_3^{2+}$-doped Xerogels: Fluorescence Lifetime Dependence on Ambient O_2 (g) Concentration

The xerogel doped with 1.0×10^{-4} M $Ru(dpp)_3^{2+}$ solution exhibited two lifetimes in air: $\tau_1 = 938 \pm 49$ ns ($\chi^2 = 1$) and $\tau_2 = 121 \pm 16$ ns ($\chi^2 = 0.9494$). These results are summarized in Table 7. The existence of two decay pathways indicates that the $Ru(dpp)_3^{2+}$ probe is proportioning into two micro-environments within the xerogel matrix. As we know that the lifetimes of the probe are affected by the presence of O_2(g), it is useful to compare the lifetimes in N_2(g) to examine the "true" probe environments. The second lifetime was much longer in N_2(g), and the first lifetime was essentially unchanged: $\tau_1 = 922 \pm 35$ ns ($\chi^2 = 0.9765$) and $\tau_2 = 5003 \pm 64$ ns ($\chi^2 = 1.008$). As in the aerogel, the shorter lifetime, τ_1, likely represents the fluorescence decay of the fluorophore in a constrained environment, whereas the longer lifetime, τ_2, may be representative of $Ru(dpp)_3^{2+}$ in a less constrained environment. Again, the effect of O_2(g) on the lifetimes was much more pronounced for the longer lifetime, indicating that it has high access to the air sample. Presumably, the probes are partitioning into the interior of the silicate matrix and along the pore-matrix interface in the xerogel and the aerogel alike. This indicates that probe partitioning occurs during the early stages of the sol-gelation process.

Table 7. Fluorescence lifetime of $Ru(dpp)_3^{2+}$ and $Ru(bpy)_3^{2+}$- doped xerogels in the presence and absence of O_2(g).

	$Ru(dpp)_3^{2+}$ -doped xerogel		$Ru(bpy)_3^{2+}$ - doped xerogel	
	Air	Nitrogen	Air	Nitrogen
τ_1 (ns)	938 ± 49	922 ± 35	521 ± 43	492 ± 32
χ^2	1	0.9765	0.9704	0.9945
τ_2 (ns)	121 ± 16	5003 ± 64	1906 ± 90	1983 ± 60
χ^2	0.9494	1.008	0.9704	0.9945

The 1.0 x 10^{-4}M $Ru(bpy)_3^{2+}$-doped xerogels also exhibited two lifetimes in air: τ_1= 521± 43 ns (χ^2= 0.9704) and τ_2= 1906 ± 90 ns (χ^2= 0.9704). These results are summarized in Table 7. The $Ru(bpy)_3^{2+}$ - doped xerogel lifetimes were essentially unchanged when deaerated with N_2(g). $Ru(dpp)_3^{2+}$-doped sol gels, on the other hand, exhibit noticeable changes in fluorescence lifetime when exposed to oxygen, again confirming the promise of $Ru(dpp)_3^{2+}$-doped sol gels as oxygen sensors.

VI. Comparing $Ru(dpp)_3^{2+}$ & $Ru(bpy)_3^{2+}$-doped Sol Gels: Differences in Probe Behavior in the Sol-gel Matrix

It is clear that the effect of oxygen quenching on $Ru(dpp)_3^{2+}$-doped sol gels is much more pronounced than the effect of oxygen quenching on $Ru(bpy)_3^{2+}$-doped sol gels, confirming that $Ru(dpp)_3^{2+}$-doped aerogels hold more promise as oxygen gas sensors. By comparing the fluorescence decay of the two systems independent of fluorescence quenching effects (Table 8), we can examine the character of the two probes within the sol gel. The second lifetime of the $Ru(dpp)_3^{2+}$-doped aerogels was much longer than that of the $Ru(bpy)_3^{2+}$-doped aerogels, indicating that the $Ru(bpy)_3^{2+}$ at the pore-matrix interface is in a more rigid environment than the $Ru(dpp)_3^{2+}$ at the pore-matrix interface. The ring system of $Ru(dpp)_3^{2+}$ is much larger than that of $Ru(bpy)_3^{2+}$, and they both have the same overall complex charge. The dispersal of charge over a larger volume could decrease the strength of the charge-charge interactions between the pore wall and the fluorophore, thereby giving $Ru(dpp)_3^{2+}$ increased freedom of motion, corresponding to a longer fluorescence lifetime. It is also likely that steric effects are contributing to the

difference in lifetimes in $Ru(dpp)_3^{2+}$ and $Ru(bpy)_3^{2+}$, as the point charges on the matrix wall may not be able to access the diffuse positive charge on the $Ru(dpp)_3^{2+}$ complex.

Table 8. Lifetimes in N_2(g) of $Ru(dpp)_3^{2+}$ & $Ru(bpy)_3^{2+}$-doped sol gels.

	$Ru(dpp)_3^{2+}$ - doped aerogel	$Ru(bpy)_3^{2+}$ - doped aerogel
τ_1 (ns)	4.601 ± 0.018	4.68 ± 0.31
χ^2	1.011	1.033
τ_2 (ns)	4851 ± 53	1583 ± 11
χ^2	1.011	1.082

	$Ru(dpp)_3^{2+}$ - doped xerogel	$Ru(bpy)_3^{2+}$ - doped xerogel
τ_1 (ns)	922 ± 35	492 ± 32
χ^2	0.9765	0.9945
τ_2 (ns)	5003 ± 64	1983 ± 60
χ^2	1.008	0.9945

VII. $Ru(dpp)_3^{2+}$- doped Aerogels & Xerogels: The Development of a Gas Sensor

The fluorescence intensity of a solution of $Ru(dpp)_3^{2+}$ in EtOH went from 7.5 x 10^5 counts/sec in an oxygen-rich environment (air) to 2.6 x 10^6 counts/sec in an oxygen-poor environment. This 3.5-fold increase in intensity required 69 minutes of deaeration, as shown in Figure 20. Figure 21 shows that the aerogel sensor fully responds to changes in ambient oxygen concentration, from an air to a 100 % nitrogen environment, within 10 seconds and with a 4.6-fold increase in signal intensity. This is a 400-fold improvement in response time that can be attributed to the low density of the aerogel. Aerogels with densities as low as 0.3 g/ cm^3 can be prepared by the Union Rapid Supercritical Extraction Method.[8] The low-density of the material allows for the rapid diffusion of

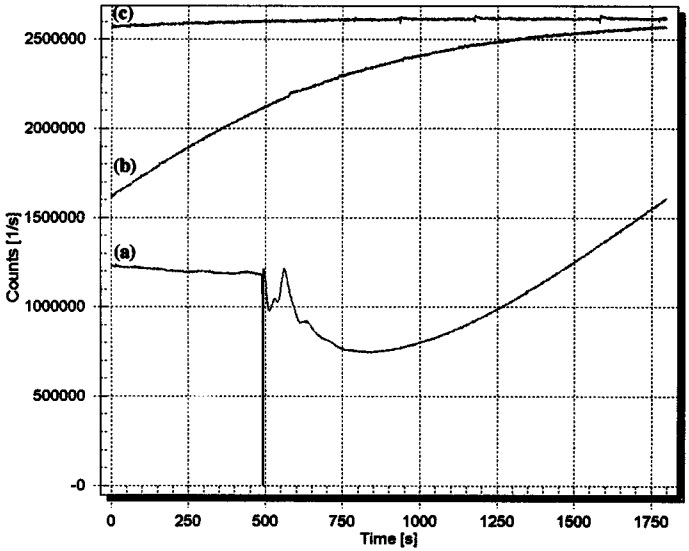

Figure 20. Fluorescence intensity v. time; the response of $Ru(dpp)_3^{2+}$ in EtOH solution to $N_2(g)$. The sample was initially deaerated by vigorously bubbling $N_2(g)$ for 8 minutes. The cap of the sample was removed at roughly 500 seconds, where there is a glitch in the signal from opening the fluorometer housing. $N_2(g)$ was then pumped into the fluorometer housing. The bottom trace (a) shows the first 30 minutes of data collection, the middle trace (b) is the second 30 minutes, and the top trace (c) shows the last 30 minutes. The signal is stable 69 minutes after the $N_2(g)$ pumping began. λ_{ex} = 446 nm, λ_{em} = 615 nm, 2 data points/s.

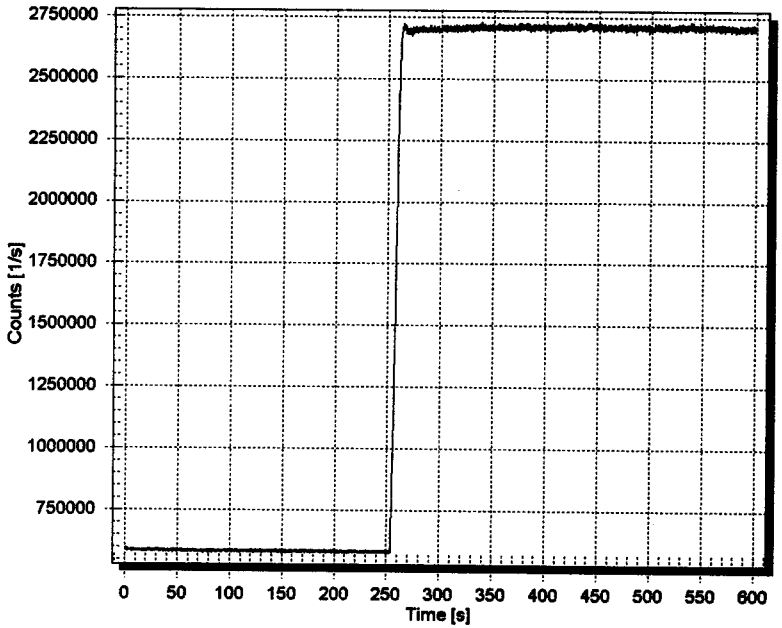

Figure 21. Fluorescence intensity v. time; the response of 1.0 x 10^{-4} M$Ru(dpp)_3^{2+}$-doped aerogel to N_2(g). The sample was initially in air under ambient conditions in an uncapped cuvette. Just after t = 250 s, N_2(g) was allowed to impinge directly onto the sample. The signal was stable within 10 s, and a 4.6 fold signal increase was observed. λ_{ex} = 446 nm, λ_{em} = 615 nm, 10 data points/s.

ambient air into the sample, giving the fluorescent probe nearly instantaneous access to the analyte. Indeed, the lifetime data indicate that the probes may be in direct contact with the sample of interest, as they seem to be partitioning along the pore-matrix interface. The rapid, reversible response renders the use of these detectors as switches very promising. Figure 22 shows the reversibility of the $Ru(dpp)_3^{2+}$-doped aerogel system.

It is unknown whether the concentration of the fluorophore in the aerogel and the solution are comparable, although a 1.0×10^{-5} M $Ru(dpp)_3^{2+}$ solution and a 1.0×10^{-5} M $Ru(dpp)_3^{2+}$-doped aerogel were used for these measurements. Because of the uncertainty of the probe concentration within the material, we compare relative changes in intensity between the oxygen-rich and oxygen-poor samples.

A similar experiment was conducted using $Ru(bpy)_3^{2+}$-doped aerogels. These aerogels also showed a rapid, reversible response, but there was only a 10% increase in signal intensity, as shown in Figure 22. The relative response of $Ru(dpp)_3^{2+}$-doped aerogels is nearly 4.2 times as strong. The $O_2(g)$ sensitivity of $Ru(dpp)_3^{2+}$, along with the ease with which this probe can be incorporated into an aerogel, makes it a superior candidate for the development of a gas sensor on an aerogel platform.

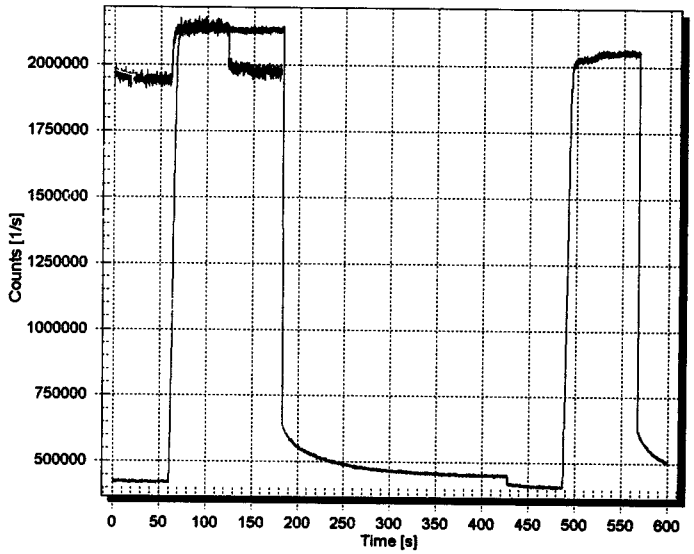

Figure 22. Reversible response of $Ru(dpp)_3^{2+}$ and $Ru(bpy)_3^{2+}$-doped aerogels to changes in ambient $O_2(g)$ concentration. The response of 1.0 x 10^{-4} M $Ru(dpp)_3^{2+}$ - doped aerogel to changes in ambient $O_2(g)$ concentration is shown in red. The sample was initially in air under ambient conditions in an uncapped cuvette. Just after t = 60 s, $N_2(g)$ was allowed to impinge directly onto the sample. The $N_2(g)$ was then shut off at 180 seconds. This process was then repeated. The signal was stable within 10 s, and a 360% signal increase was observed. The response of 1.0 x 10^{-4} M $Ru(bpy)_3^{2+}$ - doped aerogel to changes in ambient $O_2(g)$ concentration was normalized to the $Ru(dpp)_3^{2+}$ signal and is shown in blue. The signal was stable within 10 s, and a 10 % signal increase was observed. λ_{ex} = 446 nm, λ_{em} = 615 nm, 10 data pts/s.

The 10-s response time did not show improvement with the novel air-delivery system and modified cuvette cap (Figure 8). This new system requires manual adjustment of the $N_2(g)$ and air proportions. Hence, response times are variable. With the ongoing enhancement of the Union RSCE Aerogel Fabrication Method,[8,11] we may be able to obtain aerogels that are lower density and have higher surface areas. This will allow faster diffusion of fluids into the sample as well as increased fluorophore-sample contact. This could result in an improved detector response time.

A 1.0×10^{-4} M $Ru(dpp)_3^{2+}$-doped aerogel responded to changes in ambient $O_2(g)$ concentration in a non-linear fashion, as shown in Figure 23. The $Ru(dpp)_3^{2+}$-doped aerogel was highly sensitive to low $O_2(g)$ concentrations, and the signal intensity dropped to less than one-third of its maximum when going from 0 to 3% $O_2(g)$. The signal continued to decrease as the $O_2(g)$ concentration was increased from 3% to 21.5% $O_2(g)$. We then decreased the $O_2(g)$ concentration from 21.5% to 0% $O_2(g)$ and monitored the signal intensity. When these data were plotted with their standard deviations, the points fell directly on top of the first data set. Hence, the response was reversible and exhibited strong reproducibility.

We will probe the change in signal intensity from 0 to 3% $O_2(g)$ by creating gaseous mixtures with less than 3% $O_2(g)$. These mixtures could be prepared by diluting the air

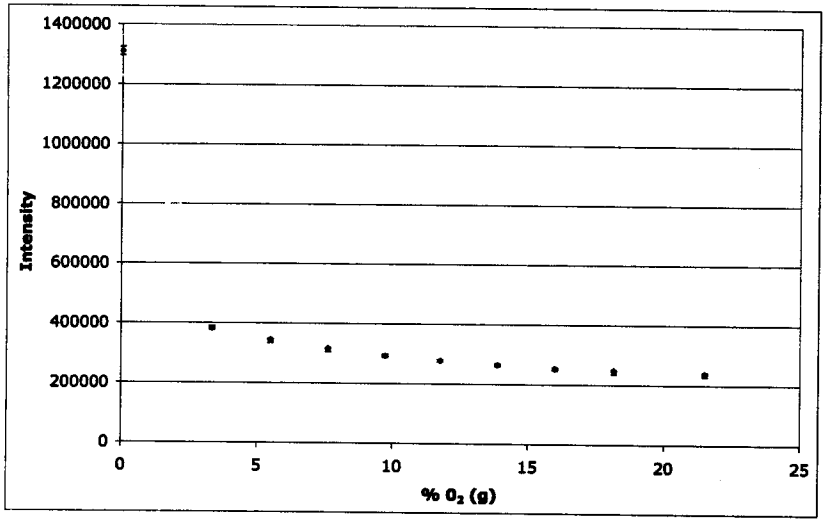

Figure 23. Fluorescence intensity as a function of ambient oxygen concentration: Calibration curve for a 1.0 x 10^{-4} M $Ru(dpp)_3^{2+}$-doped aerogel. The curve was obtained by monitoring the fluorescence intensity (λ_{ex}=446, λ_{em}=615) of the doped aerogel in different gaseous mixtures of air and N_2 (g). The blue points were obtained going from a high-oxygen to a low-oxygen environment, and the red points were obtained going from a low-oxygen to a high-oxygen environment. The error bars represent one standard deviation of the signal at each % O_2, and 4 intensities (data points) were averaged for each gaseous mixture.

samples with increased flow rates of N_2(g). A line regulator could be employed to maintain a non-destructive flow rate of fluid onto the aerogel (~1800 ml/min, 17.5 psi) in spite of the increased N_2(g) influx. Time did not allow for these trials to be conductedand included in this work, although it is possible to perform these experiments using our current gas flow system. It will be valuable to calibrate the response of multiple, simultaneously prepared aerogels, as well as aerogels prepared separately. This would allow us to evaluate sensor-to-sensor reproducibility, determine whether calibration of individual sensors would be necessary, and examine the potential commercial application of our current fabrication techniques. A calibration curve for aerogels doped with different $Ru(dpp)_3^{2+}$ concentrations could also be developed to investigate the reproducibility of the relative change in fluorescence intensity with respect to changing O_2(g) concentration.

While aerogels are very promising materials with numerous applications, they have been shown to collapse in water.[12] This severely limits the potential applications of our O_2(g) sensors, namely in the field of biosensors, as most biological systems are indeed aqueous. Some xerogels, on the other hand, perform well in aqueous environments, retaining their sensor capabilities[12] when doped with fluorescent probes using the methods described above. We tested the response of a 1.0×10^{-4} M $Ru(dpp)_3^{2+}$-doped xerogel to changes in ambient oxygen concentration, and those results are shown in Figure 24. After applying a positive pressure of N_2(g), the xerogel signal responded fully and stably after only 50 s, with a 7.25-fold signal increase. This response was also shown to be reversible.

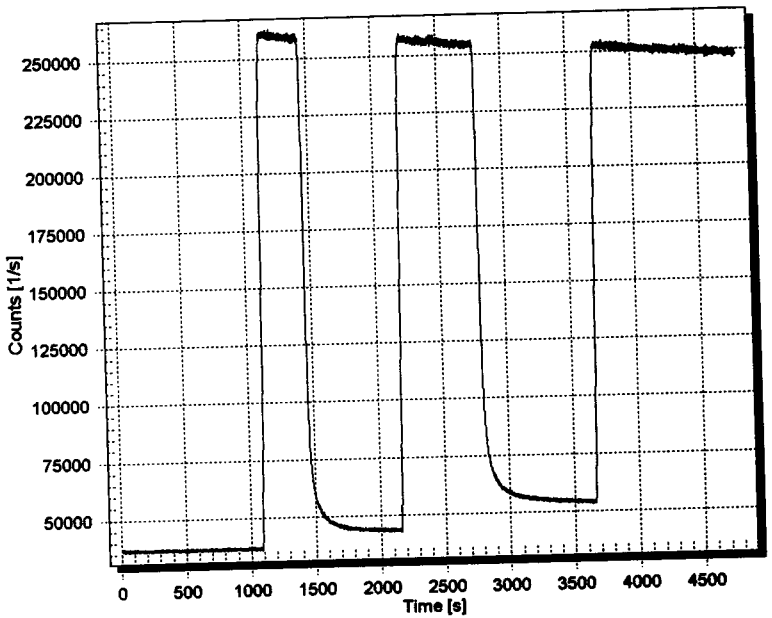

Figure 24. Reversible response of $Ru(dpp)_3^{2+}$ -doped xerogel to changes in ambient $O_2(g)$ concentration. The response of 1.0×10^{-4} M $Ru(dpp)_3^{2+}$ - doped xerogel to changes in ambient $O_2(g)$ concentration is shown in red. The sample was initially in air under ambient conditions in an uncapped cuvette. Just after t = 1100 s, $N_2(g)$ was allowed to impinge directly onto the sample. The $N_2(g)$ was then shut off at 1450 s. This process was then repeated. The signal was stable within 10 s, and a 625% signal increase was observed. $\lambda_{ex} = 446$ nm, $\lambda_{em} = 615$ nm, 2 data points/s.

It is important to note that the 50 s response time was obtained with a much lower N_2(g) flow rate than was used for the $Ru(dpp)_3^{2+}$-doped aerogel, because the sample moved out of the excitation beam when high flow rates (~1800 mL/min) were employed. This rapid response time indicates that a low density is maintained within the xerogel matrix, in spite of the collapse of the pore structure during xerogel fabrication. We predict that the rate of response of the xerogel will not differ significantly from that of the aerogel if the two were examined using the same flow rates. The more pronounced response in the xerogel (7.25-fold signal increase in the xerogel, 4.6-fold signal increase in the aerogel) may be due to differences in character of the probe within the two matrices. If the fluorophores in the aerogel are arranged in such a way that they self-quench, the effect of oxygen on the fluorophore may be decreased. If the fluorophores in the xerogel do not arrange in such a fashion, we could observe the full effects of oxygen quenching of the probe complex. Recall that the fluorescence lifetimes of $Ru(dpp)_3^{2+}$ are much longer in the xerogel than in the aerogel (Table 8), indicating that the probes are in a more constrained environment in the aerogel. It is possible that this added rigidity is arising from probe-probe interactions (i.e. aggregation, stacking) and not the sol-gel matrix.

Sol gels prepared from 1.0×10^{-5} M $Ru(dpp)_3^{2+}$ have the same emission maximum, as shown in Table 9. Xerogels and aerogels prepared from more concentrated solutions of $Ru(dpp)_3^{2+}$ do not show the same agreement. The peak emission in the aerogel occurs at 616 nm, which is red-shifted with respect to the peak emission in the xerogel (λ_{max} = 609 nm). The red-shift in the emission spectrum of the aerogel may arise from $Ru(dpp)_3^{2+}$ aggregation at higher concentration, which could decrease the overall energy of the

complex by giving it a more aromatic-like character. The presence of solvent in the xerogel could decrease probe-probe interactions, thereby preventing the aggregation and/or stacking of the $Ru(dpp)_3^{2+}$.

Table 9. Peak emission wavelengths for $Ru(dpp)_3^{2+}$ aerogels and xerogels.

$Ru(dpp)_3^{2+}$ Concentration, (M)	Xerogel	Aerogel
1.0×10^{-4} M	609	616
1.0×10^{-5} M	602	602

We recommend preparing sol gels and solutions over a range of $Ru(dpp)_3^{2+}$ concentrations, and then collecting excitation and emission spectra of those samples. Monitoring the peak intensity as a function of probe concentration would allow one to investigate the point at which stacking and/or aggregation is occurring in the samples. The intensity at the peak wavelength (λ_{max}=615 nm for $Ru(dpp)_3^{2+}$ solutions) will drop off once the probes begin aggregating into a complex with a new optimal fluorescence maximum. Understanding whether or not the probes are aggregating, as well as the effect of O_2 (g) on those probe assemblies, is essential to the interpretation of the lifetime data when comparing the xerogels and aerogels.

We do not attribute the discrepancy in signal increase between the aerogel and the xerogel to the difference in surface area of the two materials, as the relative signal increase should not be affected. That is, we should see the same relative response when going from an oxygenated to a deoxygenated system, regardless of the number of sampled fluorophores. Preliminary measurements of gas adsorption indicate that the

xerogels have a higher surface area than the aerogels prepared by the Union RSCE Method.[11] To date, we have not been able to elucidate what caused the higher surface area, and it may have simply been an anomaly. Further tests are warranted.

The ease of the fabrication process coupled with sensitive, rapid gas detection makes the $Ru(dpp)_3^{2+}$-doped sol-gel sensor very attractive for use in multiple fields and applications. Using the Union RSCE Aerogel Fabrication Method, one only needs to mix the fluorophore solution with the sol-gel precursors in order to entrap the probe within the sol-gel matrix. Our gas detector responds rapidly and reversibly to low analyte concentrations in a reproducible and easy-to-detect fashion. Going from an oxygen-poor to and oxygen-rich environment, the doped aerogel signal increases by 360% within 10 seconds, and the doped xerogel signal increases by 725% within 50 seconds. The reversibility in the aerogel is such that intensity versus $O_2(g)$ data obtained in different trials matches nearly exactly. Although the response to oxygen is not linear over the range 3% to 21.5 % $O_2(g)$, we may be able to calibrate the $Ru(dpp)_3^{2+}$-doped aerogels for use as quantitative detectors. Development of the $Ru(dpp)_3^{2+}$-doped xerogel-based gas sensor has the potential to expand the range of the oxygen-sensor applications to biological systems. In addition, advances in the Union RSCE Aerogel Fabrication Method may increase the durability of the aerogels, giving them more promise for industrial manufacture. Further work towards the development of aerogel-based gas sensors could give us the capability to detect and quantify more gas-phase compounds.

References

[1]Schumacker, P.T. *American J. of Physiol.* **2002**, 27 (5).

[2]Mountcastle, V.B. *Medical Physiology*. **1980**, C.V. Mosby Co.

[3] Various news articles listed at http://www.carbonmonoxidekills.com/carbon_monoxide_inthenews.htm, May **2003**.

[4]Dunn, B.; Zink, J.I. *Chem. Mater.* **1997**, 9, 2280-2291.

[5]Brinker, C.J.; Scherer, G.W. *Sol-Gel Science*, 1989, Academic Press.

[6]Lev, O.; Tsionsky, M.; Rabinovich, L.; Glezer, V.; Sampath, S.; Pankratov, I.; Gun, J. *Anal. Chem.* **1995**, 67 (1), 22A-30A.

[7]Pierre, A.C.; Pajonk, G.M. *Chem. Rev.* **2002**, 102, 4243-4265.

[8]Gauthier, B.M. *Development of the Union Rapid Supercritical Extraction (RSCE) Aerogel Fabrication Method*, **2002**.

[9]Keeling-Tucker, T.; Brennan, J.D. *Chem. Mater.* **2001**, 13, 3331-3350.

[10]Hrubesh, L. W. *Chemistry and Industry*, Dec 17, **1990**, p. 824-827.

[11]Bakrania, S. *Characterization of Silica-Aerogels Fabricated using a Novel Processing Technique*, **2003**.

[12]Wolfe, R.L. *Investigation of Indicators in Aerogels and Xerogels*, 2003.

[13]Sharma, A.; Schulman, S.G. *Introduction to Fluorescence Spectroscopy*, John Wiley & Sons, Inc. **1999**.

[14]Lakowicz, J.R. *Principles of Fluorescence Spectroscopy, Second Edition,* Kluwer Academic/ Plenum Publishers, **1999**.

[15]Cho, E.J. and Bright, F.V. *Anal. Chem.* **2001**, 73 (14), 3289-3293.

[16]Hara, K.; Sugihara, H.; Tachibana, Y.; Islam, A.; Yanagida, M.; Sayama, K.; Arakawa, H.; Gujihsdhi, H.; Horiguchi, T.; Kinoshita, T. *Langmuir.* **2002**, 17, 5992-5999.

[17]Carraway, E.R.; Demas, J.N.; DeGraff, B.A.; Bacon, J.R. *Anal. Chem.* **1991**, 63, 337-342.

[18]Mongey, K.F.; Vos, J.G.; MacCraith, B.D.; McDonagh, C.M.; Coates, C.; McGarvey, J.J. *J. Mater. Chem.* **1997**, 7 (8), 1473-1479.

Acknowledgements & Dedication

This work would not have been possible without the ideas, knowledge, and support of my advisor, Professor Mary K. Carroll. Her style, understanding, and wisdom are admirable. For that, I thank her.

In addition, I would like to extend thanks to the students and faculty of the Aerogel Lab at Union College. Ben Gauthier '02 showed exceptional initiative and drive to commence this work and take his fabrication techniques from concept to reality. Ann Anderson worked closely with Ben in that pursuit and has since devoted much time and effort to the successful continuation of aerogel research at Union. Smitesh Bakrania fabricated all of the samples used in this study. Without his efficiency and diligence, none of this would have been possible. Without his smile, it would not have been nearly as fun. Rebecca Wolfe contributed substantially to this work though valuable discussion and suggestion, and also through her uplifting presence and encouragement.

All of the professors of the Union College Chemistry Department must be duly thanked, as they have contributed to my education in more ways than I can describe. This department has an unparalleled standard for teaching, research, and personal investment in its students. If an award were given for "The undergraduate chemistry department that contributes most to the growth and development of young chemists," it would go to this department. Prof. Michael Hagerman deserves special thanks for essential conversation and interpretation. Kathy Ryan in the Chemistry Stockroom was very helpful in keeping

this project going with equipment support, and Meg Howley offered constant assistance in cake, conversation, digital images, and printer cartridges.

Past and present Union students where also important contributors to my general and technical education; notably, Andrew Leyhane, Tania Magoon, Mark Kostuk, Michael Webb, Jon Tower, & Robert Herbst. Jamie Iannacone, George Kosturko, Alicia Every, Tim Thomas, Rakeesh Ramakrishnan, & Peter Sage also deserve recognition for their support, inspiration, cheerfulness, spirit, and willingness to rock out whenever possible. Thanks are due to Eminem, Def Leppard, Bon Jovi, Radiohead, and RAM for keeping me going. Also to *Principessia (SLC)* for being so much like the sunshine.

I also acknowledge the financial support of the National Science Foundation- Major Research Instrumentation Grant. In addition, I would like to thank Union College for their support, both financially and otherwise, of the sciences and research.

This work is dedicated to my grandmother, Agnes Forsley, who lost her first son, Dustin, to carbon monoxide poisoning at the age of 21. Her life is an inspiration for us all.